Which Pragmatic Finite Element Human Body Model Scaling Technique Can Most Accurately Predict Head Impact Conditions in Pedestrian-Car Crashes?

Ruth Paas, Jonas Östh, Johan Davidsson

Abstract Pedestrian-to-vehicle crashes remain a world-wide health issue. Human body models (HBMs) are valuable tools for pedestrian safety-system development and evaluations. HBM biofidelity evaluation against full-scale post-mortem human subjects is crucial but challenging as common normalisation techniques enable limited adaptation for varying anthropometry, and morphing HBMs to experimental data is rarely feasible. This study evaluates the effectiveness of six pragmatic pedestrian HBM scaling techniques, focusing on head impact conditions and upper-body kinematics, using the Total Human Model for Safety (THUMS) 4.0. Upper-body 6 degrees-of-freedom kinematics prior to head-vehicle contact and head impact conditions were compared with five PMHS pedestrian experiments using a small sedan. The most accurate head impact conditions were achieved when THUMS was scaled with one z-factor adjusting its height, one x-y-factor adjusting its mass, and then translated in z-direction to adjust the pelvis height to the experimental measurements. THUMS generally reproduced head impact conditions and in-plane motions, and was numerically stable. Out-of-plane movements generally scored poorly but were small in the experiments. Accurate upper arm response was crucial for accurate head impact conditions. Possible THUMS improvements include softening the neck slightly in lateral bending and reducing resistance to upper-arm abduction, especially for large angles.

Keywords Kinematics, Pedestrian, PMHS, Scaling, THUMS

I. INTRODUCTION

Pedestrian-car crashes are a persistent threat to life [1]. In these crashes, head injuries are the single most common cause of death and a source of long-term disability [2,3]. In the future, pedestrian-car exposure is expected to rise [4] while advances in technology such as autonomous vehicles and futuristic front shapes pose new possibilities for the development of pedestrian safety systems. The risk and severity of head injuries during pedestrian-vehicle impacts is known to be largely dependent on head impact conditions and the impacted surface. An important requirement for pedestrian human body models (HBMs) is therefore to predict accurate head impact conditions such as head impact velocity and head impact location on the vehicle. Head rotation is known to be a major source of traumatic brain injury (TBI) [5,6]. The importance of high-quality and biofidelic tools such as HBMs to design and evaluate pedestrian safety systems is therefore evident. Such tools need to be evaluated, e.g., by comparing their responses with those of post-mortem human subjects (PMHSs).

The pedestrian finite element (FE) HBM Total Human Model of Safety (THUMS) is a tool for development of pedestrian safety systems and frequently used by both researchers in universities and industry [7]. In its version 4.0, the kinematic response on full-scale level has been evaluated to some extent [8-10]. These evaluations compared the model with responses of three PMHSs impacted at 40 km/h by a sedan, an SUV and a minivan. Only 2-dimensional trajectories were assessed of the head, T1, L5/S1 and impacted knee and ankle/heel, impact locations on the vehicle, and injuries to the ribs, pelvis and lower extremities. No rating method was applied in these studies. The T1 and L5/S1 trajectories generally appeared to match those of the PMHSs although the head trajectories of the PMHSs were mostly flatter than those of THUMS in the later stages. Validations of the vehicle models were not published, to the best knowledge of the authors. In component testing, THUMS generally appeared to provide biofidelic responses. A list of published full-scale and component THUMS 4.0 biofidelity evaluations is already published [11]. No additional biofidelity evaluations could be found

Ruth Paas (phone: +46-31-7723647, e-mail: ruth.paas@chalmers.se) is a PhD candidate, Jonas Östh is a Researcher, and Johan Davidsson is an Associate Professor at the Department of Applied Mechanics, Chalmers University of Technology in Gothenburg, Sweden.

in literature. For pedestrian HBM evaluation, accurate prediction of head impact conditions remains crucial for head injury assessment. HBMs additionally providing accurate predictions of the overall kinematics will be very useful for new load cases, e.g., for the development and evaluation of new pedestrian safety systems.

Full-scale pedestrian experimental data publicly available for evaluation of HBM biofidelity are mainly limited to 2-dimensional kinematics (trajectories) which limits evaluating the complete 6-dimensional kinematic response of an HBM during vehicle impact. One study published 6 degrees of freedom (DOF) kinematics of the head, several vertebrae, sacrum, pelvis, and both acromia [12]. In total, five PMHSs in similar walking postures were struck laterally by a small sedan. Multiple anthropometric measurements and initial position of each subject were presented, and the influence of varying anthropometry was assessed. This study thus provided a unique data set for biofidelity evaluation of pedestrian HBMs.

Pedestrian head impact conditions and overall kinematics are known to vary substantially with the load case, pedestrian initial posture and anthropometry [12-16]. However, normalising kinematics from pedestrian full-scale experiments is challenging. Traditional methods such as momentum-based normalization methods [17,18] are not applicable for multiple dynamic impacts such as pedestrian-vehicle crashes since they require calculation of the effective mass for each impact. Traditional normalisation methods based on the total body mass [19] are of limited value for pedestrian kinematics since they do not account for the subject's height. However, subject height has been shown to affect trajectories and head impact velocity [20]. Only one pedestrian-specific normalisation method for kinematics has been published [21,22]. In this method, scaling factors based on subject body part heights were used to scale the horizontal and vertical linear displacements of each body part. However, they found apparent "evidence that the scaling methodology lacked sufficiency" [22]. Similar conclusions were drawn in other studies attempting to normalize pedestrian kinematics, e.g., [23]. Instead of normalizing pedestrian experimental kinematics, scaling HBMs to better match the experimental subjects may be a more prosperous approach.

Although morphing is currently the most accurate method to scale HBMs, existing experimental studies do not generally contain anthropometric data detailed enough to allow for morphing. Hence, the feasibility of morphing for many pragmatic applications is limited. A slightly less complex approach was taken by Watanabe et al. [10]. Before evaluating their model, they scaled body components of THUMS version 4 to all available body dimensions of the PMHS used in the comparison experiments, and adjusted the body mass. Even if a large number of body measurements is published, this approach is still not practical for many applications.

The primary aim of this study is therefore to evaluate the effectiveness of various pragmatic pedestrian HBM scaling techniques to guide future HBM evaluations, focussing on head impact conditions and whole-body 6DOF kinematics using an FE vehicle model validated for pedestrian crashes. A secondary aim is to evaluate THUMS 4.0 against a data set containing 6DOF data of the head, spine, pelvis and shoulders from five PMHSs.

II. METHODS

The THUMS model version 4.0 [24] was used to simulate five full-scale pedestrian PMHS experiments [12]. An FE vehicle model was developed and validated using impactor test data [25]. THUMS was positioned according to each experiment and then scaled using six pragmatic scaling techniques. Head and body kinematics until first head-vehicle contact were compared using the CORA rating method version 3.61 [26]. Head impact conditions, i.e., Wrap Around Distance (WAD) and head impact velocity, were assessed separately.

Experiments

Four male PMHSs of approximately average stature and one petite female PMHS (Table I) were impacted laterally by a Renault Mégane Hatchback 2004 (Figure 1) at 40 km/h. All subjects were in walking posture with the struck-side leg slightly forward (Appendix B). Maximum vehicle braking was applied 10 ms after initial contact. Braking pitch was 0.3-0.5° at pelvis impact and 0.8-1.5° at head impact. 6DOF kinematics were obtained for the head, the vertebrae T1/T2, T9/T11 and the impacted acromion. For all but one subject, 6DOF kinematics were also obtained for L2/L3/L4, the sacrum, the contralateral pelvic H-point and the contralateral acromion. For one PMHS, antero-posterior linear displacement could not be obtained. Head-impact conditions were available for all experiments. Injuries that may have affected the kinematics were an open-book pelvic fracture in the small female, possibly obtained during pelvis-vehicle impact, and a proximal comminuted open humerus fracture in one of the male subjects, obtained shortly after elbow impact against the vehicle [12].

a)

	y (mm)	-z (mm)
A	52	246
B	29	319
C	0	430
D	1	513
E	77	629
BLE	168	758
F	988	927
G	931	967

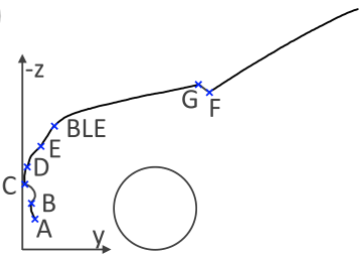

b)

Fig. 1. a) Vehicle centreline geometry, b) THUMS and FE vehicle with vehicle centre of gravity (CG, black dot)

Vehicle Model

An FE vehicle model matching the experiments was developed and validated (Fig. 1b, Appendix A) [25]. The front of a car of the same make, model and production year as used in the PMHS experiments was scanned to provide the vehicle front geometry. Material properties were largely taken from literature. For validation, the physical and the numerical vehicle were subjected to impactor tests: A rigid impactor designed to resemble a torso was dropped on the front and the rear of the bonnet. In addition, a rigid impactor simulating an upper leg was launched against the bumper, soft nose and bonnet. The final vehicle model consisted of 130 000 elements. As no data during the head impact was available from the full-scale pedestrian PMHS tests, the windscreen was modelled as a rigid surface. The front suspension was not modelled. Instead, the vehicle model was rotated by 0.5° around the vehicle's lateral axis to simulate braking pitch. Thereby, the bonnet leading edge (BLE) was lowered 14 mm which replicated the experimental BLE height at the time of pelvis impact.

Simulations

All simulations were carried out with LS-Dyna R7.1.1 [27]. Pre- and post-processing was done in LS-Prepost 4.2 [28] and Matlab R2012b [29]. THUMS was first positioned to match the posture of each PMHS. The postures were acquired from pre-test photogrammetry and measurements of body part heights and distances, replicating the head posture, shoulder level, upper body angle, extremity angles and lateral vehicle offset (Appendix B). The updated THUMS geometries were used for the following six pragmatic scaling techniques, subsequently referred to as b, t1, t2, s3, s4 and s5.

b) Baseline simulation: No scaling. The simulated floor matched the original floor height in each experiment, and THUMS was translated in such a way that the feet were in contact with the simulated floor.
t1) Translation 1: THUMS and the floor were moved to match the head CG heights in each experiment.
t2) Translation 2: THUMS and the floor were moved to match the L2/L3/L4 heights in each experiment.
s3) Scaling 3: THUMS was scaled in all three dimensions with the same factor, chosen to make the THUMS stature match those of the PMHSs. THUMS and the simulated floor were then translated to match the head CG heights measured in each experiment.
s4) Scaling 4: Two scaling factors were applied; one factor to make the stature match and another factor in the transverse plane to make the total mass match those of the PMHSs. THUMS and the simulated floor were then translated to match the head CG heights measured in each experiment.
s5) Scaling 5: Scaling s4 was applied, but THUMS and the simulated floor were translated to match the L2/L3/L4 heights measured in each experiment.

Combining the five experiments with the six scaling techniques resulted in 30 simulations. The gravitational acceleration was 9.81 m/s^2. The vehicle position and all material properties remained unchanged. The floor was shifted to 0.25 mm below THUMS, and THUMS was positioned 100 mm in front of the vehicle such that gravity brought THUMS in contact with the floor immediately prior to first THUMS-vehicle contact. Friction coefficients were 0.5 between THUMS and the vehicle, and 0.7 between THUMS and the ground [30-32].

Experiments PF02 and PM03-PM05 displayed atypical arm responses which affected the kinematics. The hand of the female PF02 was caught between the subject and the vehicle after pelvis impact, resulting in arm adduction instead of abduction at the time of elbow impact. Since this behaviour was due to subject height and posture, no constraints were added to the model. PM03 experienced an elbow impact into the windscreen and

dashboard where further elbow translation became inhibited. If the elbow impacted the windscreen in the simulations, elbow intrusion into the windscreen was allowed to the same amount as in the experiment. The elbow was then constrained to translate with the vehicle. In experiment PM04, the lycra-fabric sleeve of the ipsilateral (struck-side) arm was knotted to avoid showing the PMHS's skin. In this case, the knot became stuck between the subject's pelvis and the vehicle between the time of pelvis and elbow impact. For PM04, the upper arm motion was limited by the sleeve. Therefore, a spring was added in the simulations between the THUMS wrist and the location on the vehicle where the knot was stuck in the experiments (Appendix C2). The spring force was adjusted until the arm moved as in the experiment. PM05 received an anteriorly open, comminuted humerus fracture at and below the ipsilateral humeral head during elbow impact with the vehicle. All simulations of PM05 were restarted 5 ms after first elbow contact (Appendix C3). Prior to the restart, elements in a corresponding section of the proximal humerus and adjacent anterior soft tissue were removed.

TABLE I
EXPERIMENTAL SUBJECT DATA AND SCALING FACTORS APPLIED TO THUMS

PMHS subject number	PM01	PF02	PM03	PM04	PM05
Height (m)	1.72	1.54	1.75	1.79	1.67
Mass (kg)	69	47	88	81	68
Sex	male	female	male	male	male
Age at time of death	72	82	61	83	89
Body mass index	23.3	19.8	28.7	25.3	24.4
THUMS height scaling factor (s3-s5)	0.9768	0.8735	0.9938	1.0170	0.9881
THUMS mass scaling factor (s4-s5)	0.9815	0.8560	1.1048	1.0452	0.9690

Data Analysis and Rating

A global coordinate system according to SAE-J1733 [33] was used. Referring to the initial position of the PMHSs, the x-axis pointed in posterior-anterior direction (forward), the y-axis from left to right in the subject's lateral direction and the z-axis downward. The vehicle moved in negative y-direction. All angular displacements were calculated as successive Euler angles where x-rotation was executed first, then y-rotation, then z-rotation. All original experimental and simulation kinematics were filtered with a CFC 60 low-pass Butterworth filter [34]. The following four ratings were applied to evaluate the effectiveness of the scaling techniques (A-C) and THUMS biofidelity (D), as detailed further below:

A) Visual rating: THUMS kinematics were checked visually against those of the PMHSs
B) CORA rating: The CORrelation and Analysis (CORA) method was applied to all 6DOF displacements
C) Head impact conditions: WAD and head impact velocity were given separate scaling method ratings
D) THUMS biofidelity evaluation was done using the scaling method best rated in A-C

A) Visual rating

Visible differences between simulations and experiments, especially those deemed to considerably influence head impact conditions, were assessed in order to check whether the overall response was reasonably similar. A "poor" rating was given to simulations which displayed deviation from the experiment in two or more of the following criteria: pelvic sliding distance over the bonnet (± 15 cm), whether the head made contact with the bonnet or windscreen, upper arm abduction angle at the time of elbow impact (± 20°), elbow response following first contact with the vehicle (slipping away or staying in place), and the amount of visible support provided by the humerus to the upper torso following elbow impact. The amount of humerus support provided to the upper torso was rated "none/little" when the arm was straight, the upper arm adducted or the humerus fractured upon elbow impact, "medium" when the upper arm was abducted but slipped away after impact, or "strong" when the upper arm was abducted and the elbow stayed in place after impact.

B) CORA rating

The CORA method version 3.6.1 [35] was used to compare two curves, a simulation and an experimental curve, within a specified evaluation time period. The rating of each comparison consisted of a cross correlation and a corridor rating in order to compensate for the disadvantages of each of these methods alone [35]. For

the cross-correlation rating, CORA first shifted the experimental curve in time until the cross-correlation factor K_{xy} was maximised (Eq. 1); the shifted curve is called the cross-correlation reference.

$$K_{xy} = \frac{\sum_{i=1}^{n} x\left(t_i + \delta_{opt}\right) \cdot y\left(t_i\right)}{\sqrt{\sum_{i=1}^{n} x^2\left(t_i + \delta_{opt}\right) \cdot \sum_{i=1}^{n} y^2\left(t_i\right)}}, \quad (1)$$

where x is the value of the experimental curve at each time t_i with phase shift δ_{opt}, and y is the value of the simulation curve. From K_{xy} and δ_{opt}, a phase and a shape rating were calculated. Additionally, a size rating was calculated from the cross-correlation reference and the simulation curve. For the corridor rating, CORA constructed an inner and an outer corridor from the original, non-shifted experimental curve. From the ratings of each comparison, a total rating for each combination of experiment and scaling method was calculated.

All available 6DOF displacements were used to compare the simulations with the experiments. The end time of the evaluation interval was set to the time of first head-vehicle contact. The start of the evaluation interval was set to automatic. Thus, evaluation of each curve pair started at the time when the experimental curve reached 3 % of its maximum, removing the initial period of time when minimal displacement was observed. To reduce the influence of small displacements, the corridor size was calculated either from the maximum absolute experimental value or from a linear and angular displacement of 0.1 m and 30°, respectively, depending on which of these was the greater value. For small experimental signals (Appendix C3), the cross-correlation method was not used. Otherwise, all standard values were used as recommended [26]. For each simulation, CORA yielded a total rating and detailed ratings of each curve pair. To eliminate coincidentally high CORA scores, the total CORA rating of simulations with a "poor" visual rating was set to zero. To compare the scaling methods, a CORA scaling method rating was then calculated by averaging the total CORA ratings of each experiment for every scaling method, as CORA would have without taking poor visual ratings into account.

C) Head impact conditions

The head WAD was measured according to the Euro NCAP protocol [36] in both the experiments and the simulations. Head impact velocity was calculated as resultant head y-z-velocity relative to the vehicle and averaged over 1 ms before first head contact with the vehicle. The ratings for head WAD and head-impact velocity were calculated from the root mean square (RMS) of the relative deviation (Eq. 1),

$$R_{x,i} = 1 - RMS_{\%,x,i} = 1 - \sqrt{\frac{1}{n_i}\sum_{i}\left(\frac{x_s}{x_e} - 1\right)^2}, \quad (2)$$

where x denotes either WAD or head impact velocity; the indices s and e denote simulation and experimental results, respectively; i denotes the scaling method, and n_i is the number of results in each scaling method.

To find the best scaling method, the combined CORA ratings A and B were assessed separately from the head impact condition rating C. Higher importance was given to the rating of the head impact conditions.

D) THUMS biofidelity evaluation

The best rated scaling method was used to compare detailed THUMS responses with the experimental data. Attention was focused on head 6DOF kinematics and their boundary conditions, i.e. neck lateral bending, spine 6DOF kinematics, ipsilateral arm response and pelvic sliding over the bonnet.

III. RESULTS

Visual Rating

Of the 30 simulations, nine received a poor visual rating (Appendix C1). In the baseline simulation of PM01, the elbow remained in place following first vehicle contact instead of slipping away as it did in the PMHS experiment. The humerus then provided strong instead of medium support to the upper torso which visibly affected the head kinematics. In the baseline simulation of PF02, pelvic sliding was 17 cm instead of 0 cm in the experiment. Arm abduction was 42° larger than in the experiment since the THUMS hand was not caught between its body and the vehicle. The humerus provided medium instead of no support and the head impacted the windscreen instead of the bonnet. In simulation t2 of PF02, pelvic sliding was 20 cm larger than that of the PMHS and the head impacted the windscreen instead of the bonnet.

All six simulations of PM03 were rated as poor. In experiment PM03, the pelvis slid 45 cm and the arm abducted 73° before the elbow impacted the windscreen. Finally, the head touched the windscreen. In all PM03 simulations, sliding was only 17-22 cm and arm abduction was only 22-29°. Apart from simulation s5, the elbow never impacted the windscreen and therefore did not get pinned. In simulation s5, the elbow impacted the lower windscreen and was forced to move with the vehicle shortly thereafter. However, the arm abduction was 29° which reduced torso and head velocity somewhat but did not prevent a rather severe head impact.

All simulations of PM05 displayed arm abduction which was 40-60° smaller than the 90° abduction measured in the experiment (Appendix C1). However, all other variables were within the required ranges.

CORA Rating

Examples of CORA curve comparisons are shown in Figure 3. The head displacements of simulation s5 are compared with experiment PM04, the associated inner and outer corridors and the cross-correlation reference line as used in the CORA analysis.

In terms of whole-body kinematics, the scaling methods s3, s4 and s5 yielded the best results, followed by scaling method t1 (Table II). The baseline and t2 methods received the lowest ratings for the whole-body kinematics as they received most downgrades due to poor visual ratings.

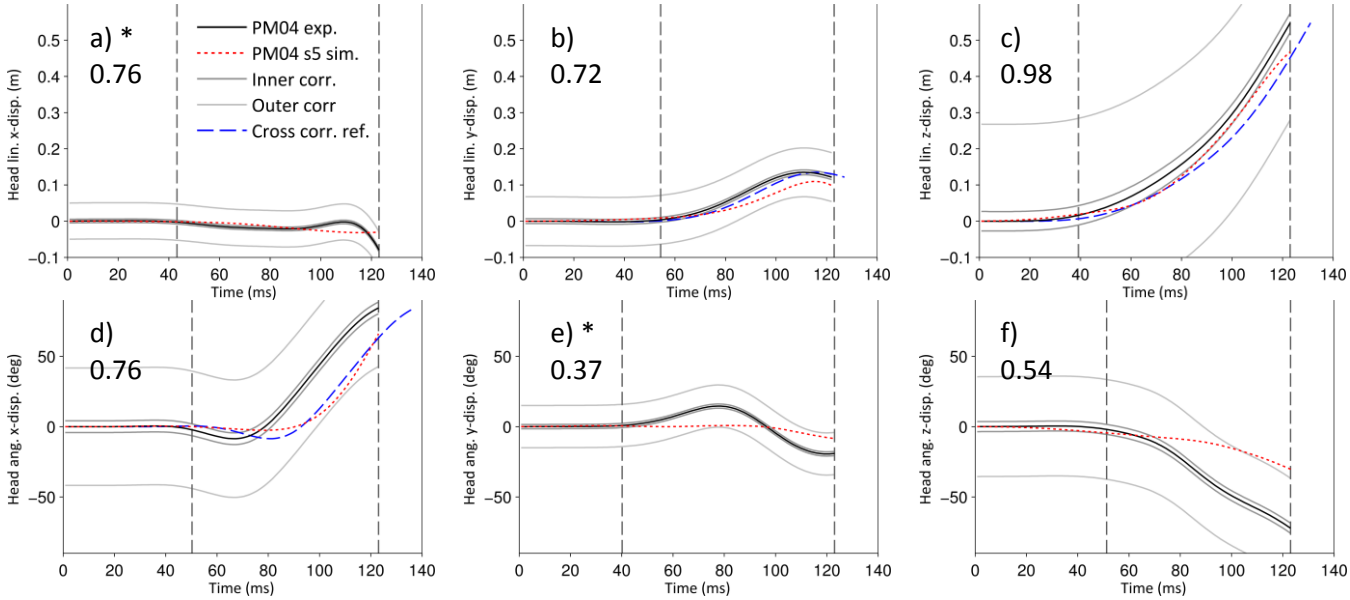

Fig. 3. Curve comparisons of head 6DOF kinematics in experiment PM04, simulation s5, with CORA ratings. Vertical dashed lines show the evaluation interval. An asterisk * indicates that the experimental maximum was below 0.1 m or 30°. For these comparisons, the corridor was widened and the cross-correlation method was not used. In Fig. 2 f), the cross-correlation reference curve coincided with the experimental curve.

TABLE II

SUMMARY OF VISUAL AND CORA RATINGS

Numbers in brackets indicate poor visual ratings that were set to zero before calculating the average rating.

Scaling	PM01	PF02	PM03	PM04	PM05	Average
b)	0 (0.58)	0 (0.50)	0 (0.63)	0.65	0.64	0.26
t1)	0.57	0.57	0 (0.64)	0.65	0.62	0.48
t2)	0.58	0 (0.62)	0 (0.62)	0.68	0.61	0.38
s3)	0.56	0.63	0 (0.62)	0.66	0.65	0.50
s4)	0.56	0.62	0 (0.62)	0.66	0.65	0.50
s5)	0.58	0.63	0 (0.60)	0.65	0.62	0.50

Head Impact Conditions

In this section, head impact locations on the vehicle, head WADs and head impact velocities are presented. PM03 was excluded from the total ratings since the head-to-windscreen contact was considered a non-typical

impact. The most accurate head impact locations on the vehicle were obtained with scaling method s5 (Fig. 4). With this scaling method, the maximum difference between simulated and experimental head WADs was 20 mm (Table III). The baseline and t2 methods yielded poor WAD results, especially for experiment PF02. WADs in the simulations of PM05 were slightly larger than in the experiment. The best head impact velocity predictions were observed with scaling method s5 (Table IV). However, the relative deviations from the experimental values were greater for the head impact velocity than for the head WADs. Consequently, the head impact velocity ratings were generally lower than the WAD ratings. Head impact velocities were generally predicted more accurately when the L2/L3/L4 height was adjusted (t2 and s5) than when the head CG height was adjusted to the experiments (t1 and s4). Head impact velocities in PM04 were consistently over 12 % smaller in the simulations than in the experiment (Appendix D2). This was partly due to the smaller neck lateral bending in THUMS than in the experiment and partly due to the upper arm response, as detailed below.

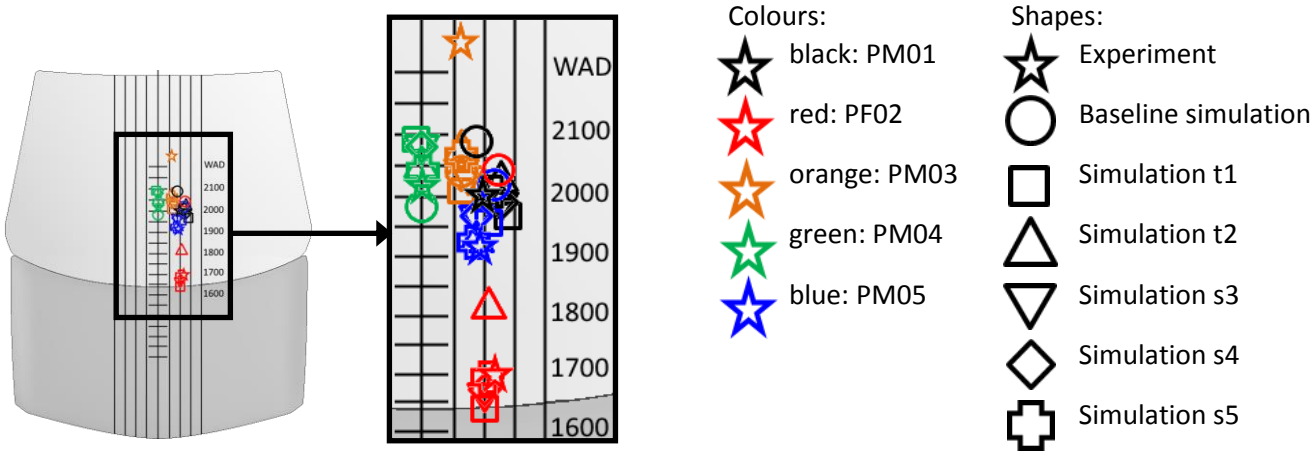

Fig. 4. Head impact locations, WAD in mm. Experimental subject PM03 experienced no severe head impact.

TABLE III
HEAD WAD RESULTS
Percentages in brackets indicate poor visual ratings. PM03 was excluded from the combined rating.

Scaling	PM01		PF02		PM03		PM04		PM05		Combined
	mm	%	mm	%	mm	%	mm	%	mm	%	$R_{WAD,i}$
Exp.	2000		1700		2250		2020		1920		
b)	2085	(+4)	2040	(+20)	2040	-9	1980	-2	2020	+5	0.89
t1)	1970	-2	1640	-4	2010	-11	2090	+4	1960	+2	0.97
t2)	2030	+2	1820	(+7)	2075	-8	2050	+1	1930	+1	0.96
s3)	1980	-1	1660	-2	2030	-10	2080	+3	1970	+3	0.97
s4)	2020	-1	1670	-2	2035	-10	2080	+3	1970	+3	0.97
s5)	2010	+1	1690	-1	2060	-8	2040	+1	1930	+1	0.99

TABLE IV
HEAD IMPACT VELOCITY RESULTS
Percentages in brackets indicate poor visual ratings. PM03 was excluded from the combined rating.

Scaling	PM01		PF02		PM03		PM04		PM05		Combined
	m/s	%	m/s	%	m/s	%	m/s	%	m/s	%	$R_{headvel,i}$
Exp.	11.0		8.7		< 1		14.5		11.8		
b)	7.1	(-35)	10.8	(+25)	9.8	(NA)	8.5	-41	9.8	-17	0.64
t1)	6.8	-38	11.7	+35	8.6	(NA)	10.6	-27	8.3	-30	0.62
t2)	12.4	+12	6.5	(-25)	13.2	(NA)	10.6	-27	11.2	-6	0.77
s3)	10.9	-1	9.3	+8	10.9	(NA)	9.5	-35	8.4	-29	0.74
s4)	8.2	-25	10.3	+19	12.1	(NA)	11.0	-25	10.6	-10	0.76
s5)	11.0	±0	9.7	+12	6.7	(NA)	12.7	-13	11.0	-7	0.89

THUMS Biofidelity Evaluation

In this section, THUMS biofidelity assessment of upper arm responses, spine, pelvis and head kinematics are presented for the s5 method only since s5 yielded the best head impact conditions and the best CORA rating.

Spine and pelvis kinematics

In the experiments, the vehicle impact against the legs and pelvis initiated leg bending, pelvis rotation and lateral bending of the lumbar spine (Fig. 5). Initially, inertia caused the upper body to remain upright and thus the thoracic and cervical spine remained straight. As the vehicle continued, the pelvis started sliding over the bonnet to varying extents. The pelvis and lower spine motion gradually induced lateral bending in the thoracic spine. When the upper thoracic spine began moving towards the vehicle, the inertia of the head caused the neck to bend laterally such that the head lagged behind the upper torso rotation towards the vehicle. In all experiments, the neck lateral bending was reduced only shortly before head impact against the vehicle. THUMS generally reproduced leg, pelvis and spine kinematics although spine and especially neck lateral bending was generally less pronounced than in the PMHSs (Fig. 5). In-plane kinematics received CORA scores of 0.74 ± 0.18.

Out-of-plane kinematics of the spine and sacrum received varying scores. Linear x-displacements were all small in the experiments (Appendix C3) and scored averages in the s5 simulations of 0.82 for T1/T2, 0.59 for T9/T11, 0.52 for L2/L3/L4 and 0.52 for the sacrum. Angular y-displacements were mostly small in the experiments and scored on average 0.34 for T1/T2, 0.51 for T9/T11, 0.53 for L2/L3/L4 and 0.42 for the sacrum. Only five of the 18 available angular z-displacements of the spine and sacrum in the experiments were small. On average, they scored 0.47 for T1/T2, 0.63 for T9/T11, 0.54 for L2/L3/L4 and 0.68 for the sacrum.

Upper arm responses

In experiments PM01 and PM03-PM05, the upper arm abducted due to inertia during the upper body rotation towards the vehicle. After elbow impact against the vehicle, the upper torso was supported by the humerus to varying extents (Appendix D1). Medium support was observed in PM01 and PM04 and virtually no support in PF02 and PM05, which was reproduced by THUMS. The strong support in experiment PM03 was not reproduced by THUMS although the upper arm support was greater in simulation s5 than in the other simulations. THUMS reproduced the experimental arm abduction but to a lesser extent, especially when the experimental arm abduction was large (73° and 90° in PM03 and PM05, respectively). In experiment PF02, the PMHS's hand was caught between the subject and the vehicle, leading to upper arm adduction instead of abduction. With method s5, THUMS reproduced this behaviour, but displayed slightly less adduction.

Head kinematics

Shoulder, arm and spine responses affected the head kinematics. In experiment PF02, the time interval between shoulder and head impact was 23 ms and thus considerably longer than in any other experiment. In experiment PF02, head resultant velocity between its peak and the head impact was reduced more than in any other experiment (Appendix C2). THUMS matched the experimental time interval between shoulder and head impact exactly in PM01, within 3 ms in PF02 and within 1 ms in PM04. In experiments PM03 and PM05, no shoulder impacts were observed due to strong arm support in PM03 and the humerus fracture in PM05.

When the humerus provided support to the upper torso after elbow contact in the experiments and s5 simulations of PM01 and PM03, the head resultant velocity was reduced prior to head impact. In PM04, limited arm abduction limited the amount of support that the humerus could provide to the torso, resulting in a comparatively high head impact velocity both in the experiment and the simulation. In PM05, the humerus did not provide much support since it fractured shortly after elbow contact. However, the upper arm remained between the vehicle and the upper torso, providing a certain amount of cushioning and reducing the head impact velocity compared with the experiment. In both the experiments and the simulations, the increasing support from the humerus or from the shoulder in PM03 and PF02 reduced the head impact velocity, but increased the head rotational velocity prior to head impact (Appendix C2).

The spine lateral bending and the head lagging behind in the experiments were generally reproduced by THUMS (Fig. 5). However, in the simulation of experiments PM04 and PM05, the head lag was less pronounced. In all simulations of these experiments, the head impact velocities were smaller than in the experiments.

CORA scores were calculated to enable a comparison between THUMS simulation and experimental head kinematics. The average CORA score was 0.72 (range 0.48-0.97) when all 6DOF displacements and all five experiments were included. Generally, the in-plane head kinematics (linear y- and z-displacement, angular x-

displacement) scored slightly higher than the out-of-plane head kinematics (Table V). However, linear x-displacements and angular y-displacements were below 0.1 m and 30°, respectively, in all experiments where these measurements were available (Appendix C2).

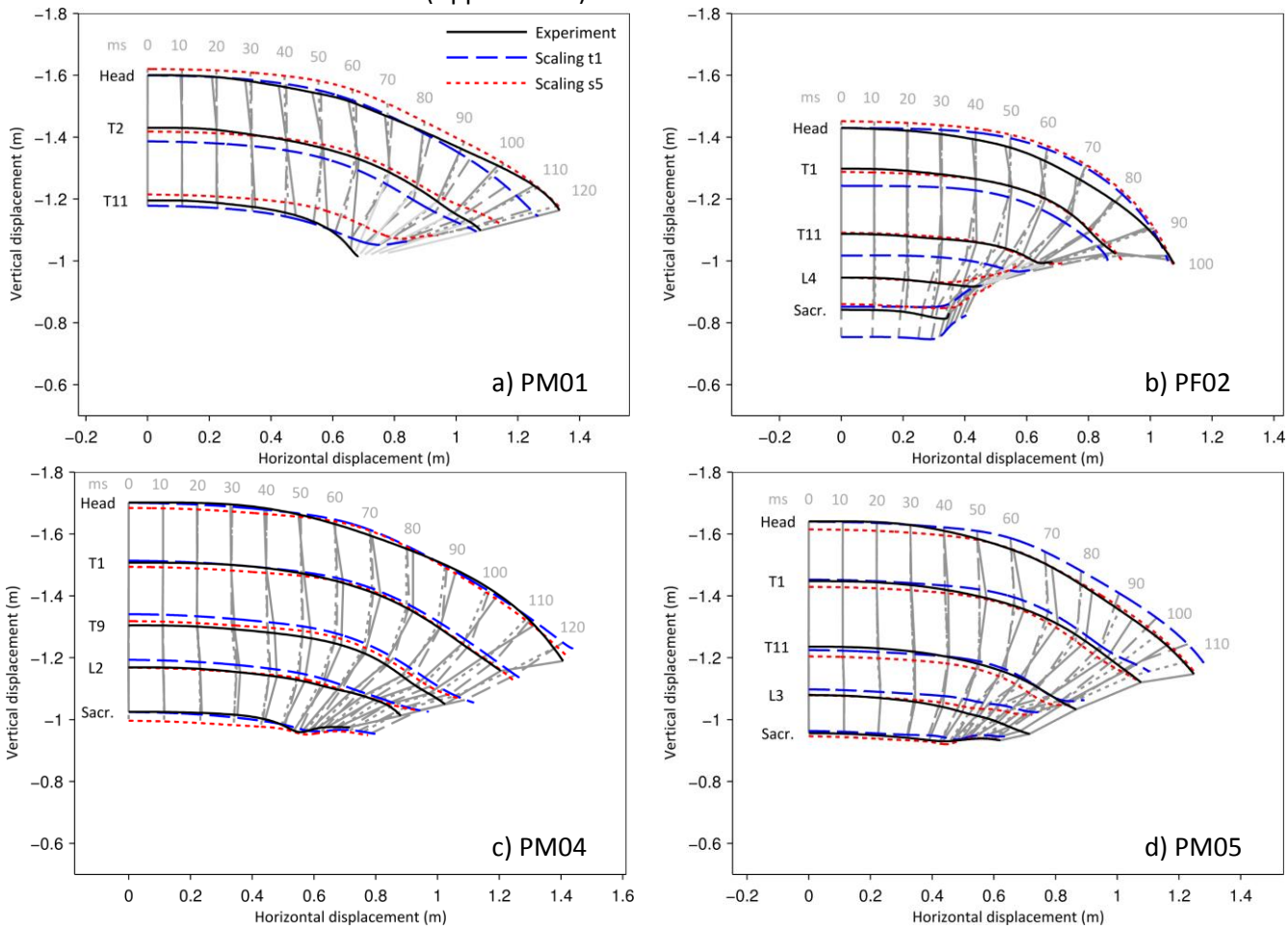

Fig. 5. Head and spine trajectories in the vehicle-fixed coordinate system. The grey lines indicate time steps of 10 ms. The amount of spine lateral bending is visualised by the angles between the grey time lines.

TABLE V
HEAD 6DOF KINEMATICS CORA SCORES IN SCALING METHOD S5
Superscript numbers show in which experiments the displacements were small.

	Lin. x-disp. [2,3,4,5]	Lin. y-disp. [1,2,3]	Lin. z-disp.	Ang. x-disp.	Ang. y-disp. [all]	Ang. z-disp. [1,3]
Average	0.57	0.61	0.85	0.69	0.38	0.47
SD	0.25	0.10	0.09	0.10	0.15	0.10
Minimum	0.32	0.48	0.73	0.59	0.25	0.33
Maximum	0.80	0.73	0.97	0.83	0.63	0.57
Median	0.58	0.65	0.85	0.69	0.35	0.50

IV. DISCUSSION

The main objective of this paper was to evaluate six pragmatic scaling techniques in terms of head impact conditions. A secondary aim was to evaluate the THUMS version 4.0 upper body response against five PMHSs.

Scaling method s5 yielded the best overall match with the experiments, i.e., the best prediction of head impact conditions and the highest CORA score. In this method, one scaling factor was used to match the stature of THUMS with the PMHSs, one scaling factor in the transverse plane to match the mass, and then THUMS was shifted to make the height of the lumbar vertebra recorded in the experiment match. Thus, this method accounted for several anthropometric factors that have been suspected to influence pedestrian kinematics and head impact conditions in previous studies. Increasing subject stature was found to increase head impact velocity and head WAD [20]. Subject mass and the height of the pelvis relative to the BLE height were suspected to change the pelvic sliding distance over the bonnet which, in turn, influenced trajectories and head

WADs [37-39]. In the experiments [12], these anthropometric factors influenced trajectories, head impact velocity and pelvic sliding. THUMS responses were sensitive to stature, mass and pelvic height. Thus, scaling method s5 was likely to provide head impact conditions most similar to those of the PMHSs. Interestingly, scaling method s5 achieved more accurate head impact velocities (rating 0.89, Table IV) and WADs (rating 0.99, Table III) than scaling method s4 (ratings 0.76 and 0.97, respectively). Shifting THUMS to make the lumbar vertebra height match (s5) thus increased the prediction accuracy over shifting THUMS to make the head CG level match that of the experiment (s4). In the visual rating, the sliding distance, the elbow WAD and the elbow abduction were generally more accurate in s5 compared with s4.

Shifting THUMS to make the lumbar vertebra height match those of the experimental subjects was an attempt to make the pelvis height match independent of pelvis geometry. Pelvis geometry varies between subjects [40]. Since no computed tomography (CT) scan was taken of the subjects in the initial positions, the height of pelvic anatomic land marks in initial position was estimated by palpation. In contrast, the vertebrae to which photo targets were firmly attached were known and their height in initial position was measured. Therefore, using the lumbar vertebra to which a photo target was attached as a reference height for shifting THUMS was deemed more accurate than using any palpated land mark on the pelvis. Sacrum photo targets were available for four out of five PMHSs. These could have been used instead of the lumbar targets. However, since the sacrum height was not measured in PM01, using sacrum target height would have led to different methods being used for the simulations of the included experiments.

The body mass index (BMI) of the experimental subjects was between 19.8 and 28.7 (Table I). Thus, no subject was underweight but two subjects could be considered overweight. However, the BMI of these subjects was higher due to a higher than average amount of muscle mass [12]. For subjects with a more extreme BMI or body proportions that are very different from that of the HBM, the scaling methods used in this study may become gradually more unsuitable. With considerably different mass distribution in the body, kinematics are expected to change in ways which the pragmatic scaling methods may not sufficiently account for. When the HBM is scaled with differing scaling factors in different directions, the element geometries may become distorted which could cause numerical instabilities. In the present study though, only four simulations were terminated due to numerical errors when negative volumes occurred in the soft tissue around the contralateral shoulder. Adding an interior contact in this part solved these errors. In addition, joint properties may change due to varying joint and ligament geometries when using highly different scaling factors in different directions. For such cases, morphing or development of a new model may be more appropriate. However, in the present study, the scaling factors in z- and x-y-direction were very similar. Thus, the effects of different scaling factors on element geometry and joint properties are expected to be small.

Several rating methods are available for HBM comparison with experimental kinematics. Vavalle et al. [41] compared three of these methods. They found that the CORA method [42] yielded the most comprehensive curve comparisons. To increase the informative value of the rating scores, Vavalle et al. [41] recommended reporting the original results to enable a more thorough examination of the curve comparisons. CORA has been used previously to evaluate the kinematics of a seated HBM [43]. For pedestrian HBM kinematics, a similar objective rating study could not be found in the literature. One advantage of CORA is that the method allows for curve-to-curve comparisons without requiring experimental corridors. Since previous attempts to normalise pedestrian kinematics have shown severe limitations [21-23], relying on experimental corridors would limit the informative value of such ratings. However, the CORA method has a number of limitations. A single rating number has limited informative value. For example, the CORA ratings in all PM03 simulations were unexpectedly good considering that the responses after elbow contact were fundamentally different from the experiment. In this particular case, CORA calculations were only done for 120-130 ms after first contact, i.e., until head-windscreen contact occurred in the simulations. This early head contact in the simulations and the fact that CORA handles missing data points by excluding them from the comparison partly explains the unexpectedly good CORA scores. PM03 was an extreme case although this issue was generally present in all CORA ratings. Shifting or scaling the time axis was considered in a way that would always include the head impact in both the experimental and simulation data. However, such an intervention would have compromised the comparability of different scaling methods. To reduce the risk of misleading CORA ratings, the visual rating was introduced and complemented with the head impact condition ratings prior to the final assessment of the

scaling methods. Using a visual rating to eliminate coincidentally high CORA ratings has not been published previously, to the best knowledge of the authors. However, this approach was preferred to adding any fundamentally different responses to the final rating.

Ipsilateral upper arm kinematics were important for the prediction of head kinematics and impact conditions. The upper arm response clearly influenced the head impact velocity. Generally, the stronger support the upper arm provided to the upper torso, the lower was the observed head impact velocity. THUMS arm abduction in PM01, PM03 and PM05 at the time of elbow impact was generally less pronounced than that of the PMHSs. When these abductions were lower than 45° in the experiment, the model simulated the response within 20° which did not appear to considerably affect the head kinematics (Appendix C). However, the large arm abductions of 73° and 90° in experiments PM03 and PM05, respectively, were not reproduced by the model. Reasons for this difference could either be a different mass distribution in the subjects compared with THUMS, or that the THUMS shoulder is slightly too stiff in abduction, especially for large angles.

In experiment PM03, the elbow was pinned in the windscreen. The upper arm subsequently provided strong support for the upper torso such that the head-windscreen contact was much less violent than in the other experiments. In all PM03 simulations, the upper arm provided much less support and impacted against the bonnet in all simulations apart from s5 where it impacted against the lower end of the windscreen. The elbow impact location differed from the experiment partly because of pelvic sliding and upper arm abduction. Arm abduction in the simulations was 24-29° (73° in the experiment). In the simulations, pelvic sliding over the bonnet until head contact was 17-22 cm; in the experiment, it was 45 cm. Partly, this difference was due to the timing of the head contact. In simulation s5, the head made contact with the vehicle 138 ms after initial contact. By that time, the PMHS in the experiment had slid 30 cm which was still 8 cm more than in simulation s5 (Appendix C). However, it was mainly due to the difference in upper arm abduction that the upper arm support differed. The differing amount of arm support resulted in the head impact velocity being considerably higher (6.7-13.2 m/s) in the six PM03 simulations than in the experiment (< 1 m/s).

In experiment PM04, a knot on the lower end of the ispilateral sleeve limited the upper arm abduction. In the simulations, a spring force of 200 N was applied to mimic the sleeve and reproduce the PMHS upper arm response. Adding the effect of the sleeve led to more accurate head impact velocity prediction (Appendix D2).

A proximal open humerus fracture in PM05 during elbow contact with the vehicle was simulated by removing upper arm elements 5 ms after first elbow contact. This improved the head impact condition predictions compared with not simulating the fracture or simulating the fracture at an earlier time point (Appendix D3). However, the WAD was still slightly larger and the head impact velocity lower in all simulations, indicating that upper arm support may still have provided stronger upper torso support than in the experiment.

The initial posture of the PMHSs was reproduced by matching THUMS posture with pre-test photos and measurements. Since no CT scan was available of the PMHSs in initial posture, the best posture match had to be estimated from pre-impact photos and measurements as accurately as possible. Initial posture angles were reproduced within 5° (Appendix B). The influence of initial posture on the results was estimated by comparing the head impact conditions of all baseline simulations which only differed by initial posture. Head WAD and head impact velocity results for the baseline ranged from 1980-2085 mm and 7.1-10.8 m/s, respectively. When excluding PM03 from the analysis, the head WAD range in the baseline simulations was relatively small compared with that in the experiments (1700-2020 mm). Head WAD appeared to be more affected by subject height and scaling method than by initial posture. The head impact velocity range in the baseline simulations was smaller than that in the experiments (8.7-14.5 m/s). Thus, although the initial posture considerably affected head impact velocity, the scaling method appeared to affect the head impact velocity to a larger extent. Considerable variation in head impact velocity was found when varying the gait in previous studies, too [44]. Considering the effect of initial posture on head impact velocity, the s5 simulations reproduced the experimental head impact velocities unexpectedly well. The positioning of THUMS thus was quite accurate.

Experimental limitations are subject embalmment and release time. The PMHSs were embalmed with a Winckler's solution [45]. The effect of this treatment on the kinematics is still debated. In addition, some variation in the release time of the subjects was noted in the experiments. However, during the time period in which the release time varied, neither experiment nor any THUMS simulation displayed any head displacement.

Limitations of this study were a limited number of test conditions. There were only five subjects tested with

only one small sedan vehicle. The best suitable pragmatic scaling method might be different for different vehicles or, as discussed previously, for considerably different mass distribution in the human body. Until the effect of these factors is examined, the conclusions of this study should be applied to similar load cases. An additional limitation was that THUMS was compared with PMHSs as opposed to living subjects. While the use of PMHSs instead of volunteers is a general limitation for pedestrian full-scale experiments, living subjects likely display somewhat different kinematics due to the effect of muscle activation and tissue properties. However, some muscle stiffness appears to be included in THUMS [11]. In actual pedestrian crashes, the amount of muscle activation may vary depending on whether or not the pedestrian is aware of an imminent crash. In the future, two versions of THUMS may be developed to simulate unaware and aware pedestrians. An additional limitation was the large effect of upper arm response on the head kinematics. However, the PMHSs' upper arm responses were generally biofidelic with the given initial postures and boundary conditions apart from experiments PM03 and PM05 where arm abduction was large (Appendix C1). These two experiments did not considerably influence the scaling method assessment since PM03 was largely excluded from the final rating, and excluding PM05 would not have changed the final conclusion. In addition, the visual rating showed that the scaling method s5 generally appeared to produce the most biofidelic THUMS responses, partly because lower and upper arm responses were replicated most accurately. Generally, the assessment of THUMS biofidelity and the assessment of the best scaling method are interconnected to some extent since there are no established scaling laws for pedestrian kinematics or experimental corridors for various pedestrian sizes available to date. In fact, within the limitations of this study, THUMS responses are most biofidelic when applying s5 scaling.

Future work will include a study into possible improvements of the THUMS arm and spine responses. To improve THUMS upper arm abduction, a number of possible factors should be considered. The pectoralis major muscle could be too stiff and not allow for an extensive enough arm abduction range of motion. The soft tissue on the inferior part of the shoulder between the proximal humerus and the thorax could be too stiff in tension. Finally, the ligaments and glenohumeral capsule should be investigated for their contribution to arm abduction. The neck should be made slightly softer in lateral bending to reproduce head lag more accurately. Another study should compare the THUMS responses after using the scaling methods from the present study with those after morphing THUMS. Several studies have compared THUMS with biomechanical data. However, validation is an on-going process in view of new experimental data and future vehicle fronts.

V. CONCLUSIONS

Scaling method s5 achieved the most accurate prediction of the head impact conditions when using a small sedan. In s5, two scaling factors were applied to match the height and mass to those of the PMHSs, and THUMS was shifted to make the height of the lumbar vertebra match. With the s5 method, THUMS generally reproduced the head impact location and head impact velocity and was also numerically stable.

Accurate reproduction of the upper arm response was crucial. For two of the five experiments, model adjustments were made to simulate a humerus fracture and a sleeve influencing upper arm response. Generally, THUMS upper arm abduction was less pronounced than that of the PMHSs, especially when arm abduction was large in the PMHSs. The amount of abduction and the elbow response after impact influenced how much support the humerus provided to the upper torso which, in turn, influenced the head kinematics. Neck lateral bending was slightly less pronounced in THUMS than in the experiments which produced slightly lower head impact velocities in some simulations compared with the experiments. Out-of-plane motions were reproduced less accurately than in-plane motions although they were generally small in the experiments. In summary, THUMS version 4.0 with s5-scaling appeared to be generally representative of a pedestrian of its size and anthropometry although minor improvements of the arm and spine responses should be considered.

Future studies should look into possible model improvements and further validate THUMS. Pragmatic scaling and morphing should be compared both for THUMS and other pedestrian HBMs.

VI. ACKNOWLEDGEMENTS

This work was funded by SAFER – Vehicle and Traffic Safety Centre at Chalmers, Sweden. The simulations were conducted on computational resources provided by the Swedish National Infrastructure for Computing (SNIC) at the Chalmers Centre of Computational Science and Engineering (C3SE).

VII. REFERENCES

[1] WHO. Global Status Report on Road Safety 2013: Supporting a Decade of Action. 2013a, World Health Organization (WHO): Geneva, Switzerland.

[2] Lau, G., Seow, E., and Lim, E.S. A review of pedestrian fatalities in Singapore from 1990 to 1994. *Ann Acad Med Singapore*, 1998. 27(6): p. 830-837

[3] Strandroth, J., Sternlund, S., Lie, A., and Tingvall, C. Correlation between Euro NCAP pedestrian test results and injury severity in injury crashes with pedestrians and bicyclists in Sweden. *Stapp Car Crash J*, 2014. 58: p. 213-231

[4] Hedlund, J. Pedestrian Traffic Fatalities by State. 2010, Governors Highway Safety Association: Washington, DC.

[5] Holbourn, A.H.S. The mechanics of head injuries. *The Lancet*, 1943. 2(6267): p. 438-441

[6] Kleiven, S. Predictors for traumatic brain injuries evaluated through accident reconstructions. *Stapp Car Crash J*, 2007(51): p. 81-114

[7] Yasuki, T. Using THUMS for pedestrian safety simulations. *ATZ Auto Technology*, 2006. 6(4): p. 44-47

[8] Shigeta, K., Kitagawa, Y., and Yasuki, T. Development of next generation Human FE Model capable of Organ Injury Prediction. *Proceedings of ESV Conference*, 2009. Stuttgart, Germany

[9] Watanabe, R., Miyazaki, H., Kitagawa, Y., and Yasuki, T. Research of Collision Speed Dependency of Pedestrian Head and Chest Injuries using Human FE Model (THUMS Version 4). *Proceedings of ESV Conference*, 2011. Washington, D.C.

[10] Watanabe, R., Katsuhara, T., Miyazaki, H., Kitagawa, Y., and Yasuki, T. Research of the Relationship of Pedestrian Injury to Collision Speed, Car-type, Impact Location and Pedestrian Sizes using Human FE model (THUMS Version 4). *Stapp Car Crash J*, 2012. 56 (October 2012): p. 269-321

[11] Paas, R., Davidsson, J., and Brolin, K. Head kinematics and shoulder biomechanics in shoulder impacts similar to pedestrian crashes – a THUMS study *Traffic Inj Prev*, 2015. 16(5): p. 498-506

[12] Paas, R., Masson, C., and Davidsson, J. Head boundary conditions in pedestrian crashes with passenger cars: six-degrees-of-freedom post-mortem human subject responses. *Int J Crashworthiness*, in press

[13] Kerrigan, J.R., Arregui, C., and Crandall, J.R. Pedestrian Head Impact Dynamics: Comparison of Dummy and PMHS in Small Sedan and Large SUV Impacts. *Proceedings of ESV Conference*, 2009. Stuttgart, Germany

[14] Thollon, L., Jammes, C., et al. How to Decrease Pedestrian Injuries - Conceptual Evolutions Starting From 137 Crash Tests. *The Journal of Trauma - Injury, Infection, and Critical Care* 2007. 62(2): p. 512-519

[15] Kallieris, D. and Schmidt, G. New Aspects of Pedestrian Protection Loading and Injury Pattern in Simulated Pedestrian Accidents. *SAE Technical Paper 881725*, 1988

[16] Kendall, R., Meissner, M., and Crandall, J. The Causes of Head Injury in Vehicle-Pedestrian Impacts: Comparing the Relative Danger of Vehicle and Road Surface. *SAE Technical Paper 2006-01-0462*, 2006

[17] Mertz, H.J. A Procedure for Normalizing Impact Response Data, in *SAE Technical Paper 840884*. 1984.

[18] Viano, D.C. Biomechanical Responses and Injuries in Blunt Lateral Impact. *Proceedings of Stapp Car Crash Conference*, 1989. Washington, DC

[19] Eppinger, R.H., Marcus, J.H., and Morgan, R.M. Development of Dummy and Injury Index for NHTSA's Thoracic Side Impact Protection Research Program. *SAE Technical Paper 840885*, 1984

[20] Okamoto, Y., Sugimoto, T., Enomoto, K., and Kikuchi, J. Pedestrian head impact conditions depending on the vehicle front shape and its construction--full model simulation. *Traffic Inj Prev*, 2003. 4(1): p. 74-82

[21] Kerrigan, J.R., Kam, C.Y., et al. Kinematic Comparison of the Polar II and PMHS in Pedestrian Impact Tests with a Sport-Utility Vehicle. *Proceedings of IRCOBI Conference*, 2005b. Praque, Czech Republic

[22] Kerrigan, J.R., Crandall, J.R., and Deng, B. Pedestrian kinematic response to mid-sized vehicle impact. *Int J Veh Saf*, 2007. 2(3): p. 221-240

[23] Untario, C., Shin, J., et al. A study of the pedestrian impact kinematics using finite element dummy models: the corridors and dimensional analysis scaling of upper-body trajectories. *Int J Crashworthiness*, 2008. 13(5): p. 469-478

[24] TMC. THUMS User Manual, AM50 Pedestrian/Occupant Model, Academic Version 4.0_20111003. 2011, TOYOTA MOTOR CORPORATION.

[25] Paas, R. and Davidsson, J. Development and validation of a Renault Mégane finite element model for full-scale pedestrian impact simulations. 2015, Chalmers University of Technology: Göteborg, Sweden.

[26] Thunert, C. CORA Release 3.6 User's Manual. 2012, PDB - Partnership for Dummy Technology and Biomechanics: Ingolstadt / Braunschweig, Germany.
[27] LSTC Inc. LS-Dyna R7.1.1. 2014a: Livermore, CA.
[28] LSTC Inc. LS-Prepost 4.2. 2014b: Livermore, CA.
[29] Mathworks, T. MATLAB R2012b. 2012: Natick, MA.
[30] Carter, E., Ebdon, S., and Neal-Sturgess, C. Optimization of Passenger Car Design for the Mitigation of Pedestrian Head Injury Using a Genetic Algorithm. *Proceedings of GECCO*, 2005. Washington DC
[31] Yang, J.K., Lövsund, P., Cavallero, C., and Bonnoit, J. A Human-Body 3D Mathematical Model for Simulation of Car-Pedestrian Impacts. *Journal of Crash Prevention and Injury Control*, 2000. 2(2): p. 131-149
[32] Bhalla, K., Montazemi, P., and Crandall, J. Vehicle impact velocity prediction from pedestrian throw distance: Trade-offs between throw formulae, crash simulators and detailed multi body modelling. *Proceedings of IRCOBI Conference*, 2002. Munich, Germany
[33] SAE. J1733 - Sign Convention for Vehicle Crash Testing. Issued DEC94. 1994, Society of Automotive Engineers, Inc. (SAE): Warrendale, PA.
[34] SAE. J211 - Instrumentation for Impact Test - Part 1 - Electronic Instrumentation. 1995, Society of Automotive Engineers, Inc. (SAE): Warrendale, PA.
[35] Gehre, C., Gades, H., and Wernicke, P. Objective Rating of Signals using Test and Simulation Responses. *Proceedings of ESV Conference*, 2009. Stuttgart, Germany
[36] Euro NCAP. Pedestrian Testing Protocol. 2014, European New Car Assessment Programme (Euro NCAP).
[37] Anderson, R.W.G., Streeter, L.D., Ponte, G., and McLean, A.J. Pedestrian reconstruction using multibody MADYMO simulation and the Polar-II dummy: a comparison of head kinematics. *Proceedings of ESV Conference*, 2007. Lyon, France
[38] Kerrigan, J.R., Murphy, D.B., et al. Kinematic Corridors for PMHS Tested in Full-Scale Pedestrian Impact Tests. *Proceedings of ESV Conference*, 2005a. Washington D.C., US
[39] Subit, D., Kerrigan, J., et al. Pedestrian-Vehicle Interaction: Kinematics and Injury Analysis of Four Full-Scale Tests. *Proceedings of IRCOBI Conference*, 2008. Bern, Switzerland
[40] Segebarth-Orban, R. An evaluation of the sexual dimorphism of the human innominate bone. *J. Hum. Evol.*, 1980(9): p. 601-607
[41] Vavalle, N.A., Jelen, B.C., Moreno, D.P., Stitzel, J.D., and Gayzik, F.S. An Evaluation of Objective Rating Methods for Full-Body Finite Element Model Comparison to PMHS Tests. *Traffic Inj Prev*, 2013. 14(sup1): p. S87-S94
[42] Gehre, C., Gades, H., and Wernicke, P. Objective rating of signals using test and simulation responses. *Proceedings of ESV*, 2009. Stuttgart, Germany
[43] Park, G., Kim, T., Crandall, J.R., Arregui-Dalmases, C., and Luzon-Narro, J. Comparison of Kinematics of GHBMC to PMHS on the Side Impact Condition. *Proceedings of IRCOBI Conference*, 2013. Gothenburg, Sweden
[44] Elliott, J.R., Simms, C.K., and Wood, D.P. Pedestrian head translation, rotation and impact velocity: The influence of vehicle speed, pedestrian speed and pedestrian gait. *Accident Anal Prev*, 2012b. 45: p. 342-353
[45] Winckler, G., "Manuel d'anatomie topographique et fonctionnelle". 2 ed. 1974, Paris, France: Masson.
[46] Bosch, "Automotive Handbook". 5 ed, ed. H. Bauer. 2000, Warrendale, PA: Society of Automotive Engineers (SAE).
[47] Pipkorn, B., Forsberg, C., et al. Development and Component Validation of a Generic Vehicle Front Buck for Pedestrian Impact Evaluation. *Proceedings of IRCOBI Conference*, 2014. Berlin, Germany

VIII. APPENDIX

Appendix A – Vehicle Model

In this section, a summary of the development and validation of the FE vehicle model used in the present study is provided. A full report can be found online [25]. The vehicle model was developed and validated in order to enable simulations of previously published PMHS pedestrian experiments. Subsequently, the FE vehicle model will be referred to as "vehicle model" while the actual physical vehicle will be referred to as "physical vehicle".

Model Development

The outside geometry of the vehicle model was measured combining two sources. A detailed laser scan of the physical vehicle was conducted at Cascade (Mölndal, Sweden) which included the exterior of the front, the interior of the bonnet and, to a certain extent, the parts underneath the bonnet. The laser scan did not include the windscreen. The windscreen geometry was carefully measured by hand. For comparison of the outside geometry, a FARO arm measurement (FARO Technologies, Inc., Lake Mary, FL) of the exterior of the physical vehicle used in the PMHS tests was made with a density of 10 mm x 10 mm and a measurement error of below 2 mm. Behind the bumper as visible from the outside, a honeycomb-like plastic structure is installed to absorb energy in front of a near-rigid aluminium beam. Further upwards, behind the soft nose, a T-shaped plastic part is installed. These two plastic structures and the aluminium beam were measured by hand. The geometries of the different parts were imported or drawn in AutoCAD (Autodesk Inc.) with somewhat simplified surfaces, then slightly adjusted to ensure that they fit together as in the physical vehicle and imported into LS-Prepost 4.2. All geometries were meshed with an element size of 10 mm unless smaller elements were deemed necessary for adequate model behaviour. Material properties and part thicknesses were measured wherever possible, or obtained from literature [46,47] (references used in the Appendix are listed at the end of the document). The only exception was the thickness of a part extruded backwards from the lowest end of the front. Since there were no experimental tests available to tune or validate this part of the vehicle, this thickness was adjusted in several test simulations with THUMS in order to match the deformation of the lowest area of the front and lower leg response to those recorded in the PMHS tests. The final vehicle model consisted of 130 000 elements in 16 parts (Figure A-1).

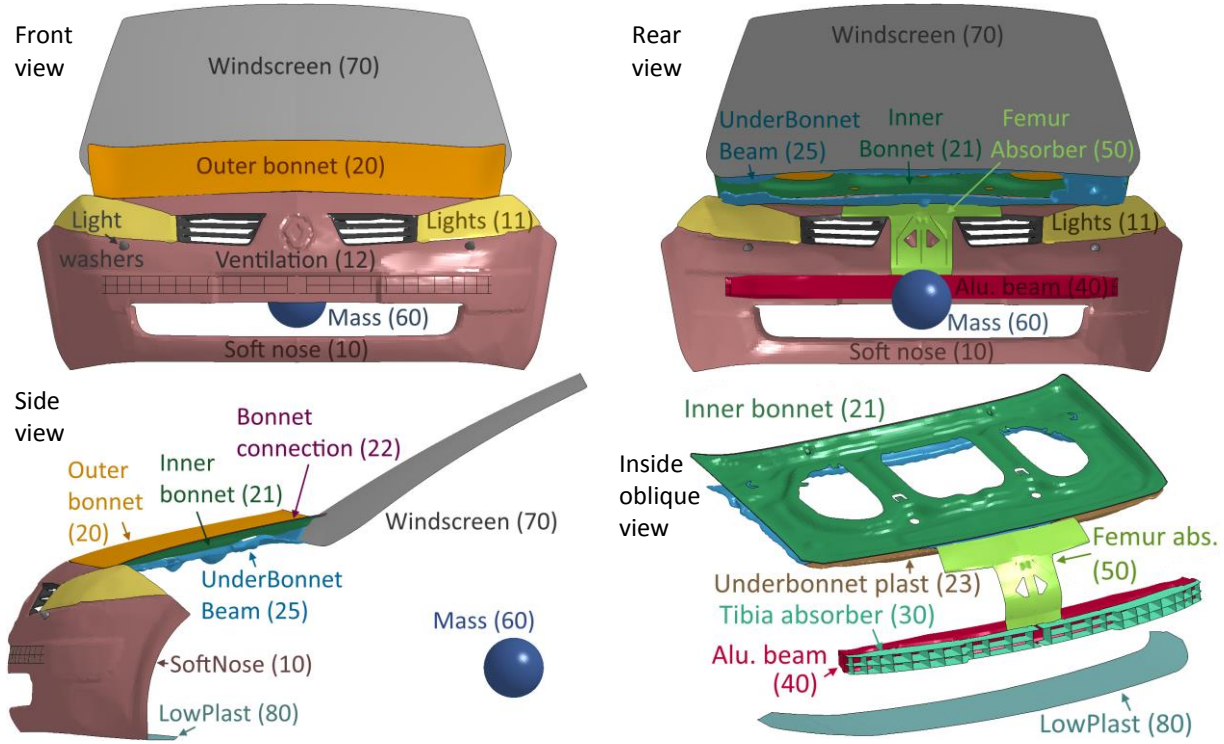

Fig. A-1. Vehicle model with part names and numbering

Model Validation

For model validation, the physical and the numerical vehicle were subjected to two series of impactor tests. In series A), a rigid impactor designed to resemble a torso was dropped on the front and the rear of the bonnet. In series B), a rigid impactor representative of an upper leg was impacted against the bumper, soft nose and bonnet.

In series A), the bonnet was tested separately. An aluminium impactor resembling a hollow, elliptic half-cylinder, representing a torso impactor, was dropped onto the rear and the front-end of the bonnet (Figure A-2). The mass of the impactor was 12 kg and the impact speed was 6.1 m/s. Displacements were measured with two string pots and by video analysis of two targets, one attached to the bonnet, one attached to the impactor. The mounting and guiding of the impactor was aimed at inhibiting rotation of the impactor. However, the videos of the experiments showed that there was some rotation present during impact in the experiments. In the impact against the rear end of the bonnet, the impactor rotation influenced the results as follows: Both experimental photo targets showed more displacement than they would have without the rotation. The experimental rear string pot displayed slightly more displacement than it would have without rotation, and the experimental front string pot displayed slightly less displacement. In the impact against the front end of the bonnet, both experimental photo targets displaced less displacement than they would have without impactor rotation. The experimental rear string pot showed slightly more and the experimental front string pot showed slightly less displacement than they would have without the rotation.

Simulations of these tests were carried out by positioning the bonnet and impactor models according to the experiments. Constraints were applied that mimicked the experimental test set-up. In the simulations, rotation of the impactor was completely restricted as the effect of the mounting and guiding could not be modelled.

The results of the experimental and simulation displacements are shown in Figure A-2. Considering how the rotation affected the displacement in the experimental tests, the FE vehicle model of the bonnet yielded reasonably good results in terms of maximum displacements.

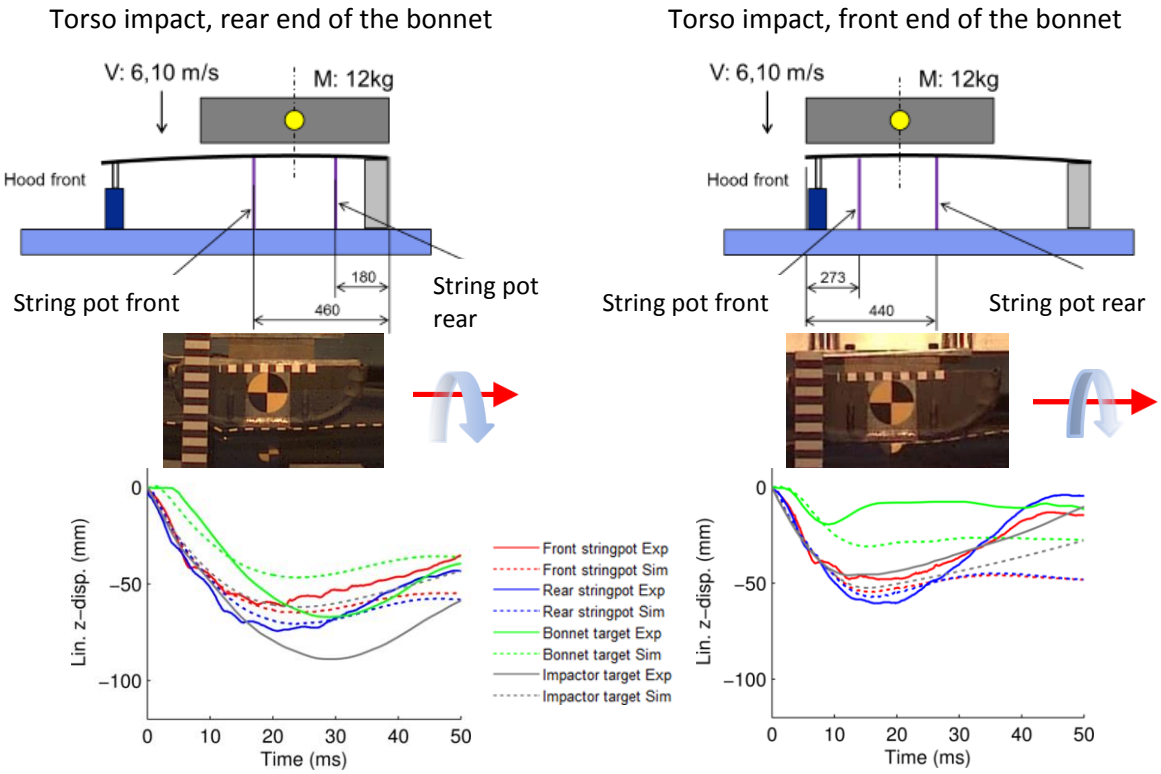

Fig. A-2. Test series A), torso impactor against bonnet. Left: impact against the bonnet rear end, Right: impact against the bonnet front end. Top: test set-up, middle: photos from the experiments with arrows showing the direction of rotation, bottom: experimental and simulation results for test series A).

In test series B), a hollow aluminium half-cylinder representing an upper leg was launched against the centre line of the vehicle front end at different angles and heights and at an impact speed of 11.1 m/s (Table A-1). The mass of the impactor was varied between 5 kg, 7.5 kg and 12 kg. The impactor was mounted on a sled which limited rotation and movement perpendicular to the impact direction. However, in experiments B3-B5, some unwanted vertical impactor movement was observed. In experiment B4, the vehicle additionally moved downwards due to engagement of the front suspension. Experimental results were impactor displacements in impact direction (y) and in vertical direction (z).

TABLE A-1
TEST MATRIX IN VEHICLE VALIDATION EXPERIMENTS, TEST SERIES B

Test no.	Car angle	Impactor angle	Impactor mass (kg)		Remarks
B1	22	0	5		No unwanted z-motion or impactor rotation observed
B2	0	0	5		No unwanted z-motion or impactor rotation observed
B3	0	30	7.5		Some unwanted z-motion of the impactor observed in the experiments (before, during and after impact)
B4	22	30	12		Some unwanted z-motion of the impactor observed in the experiments (before, during and after impact). Additionally, the vehicle was pushed downwards in the experiments, which was not simulated.
B5a, B5b	0	60	7.5		Impactor mounting expected to strongly influence impactor deceleration, could not be simulated properly. B5a and B5b displayed rather different amounts of displacement.

In the simulations of test series B, the impactor was constrained such that rotation was not allowed. In addition, the vehicle centre of gravity was fixed in space and suspension was not modelled. The results show a fairly good match between the experiment and the simulations (Figure A-3).

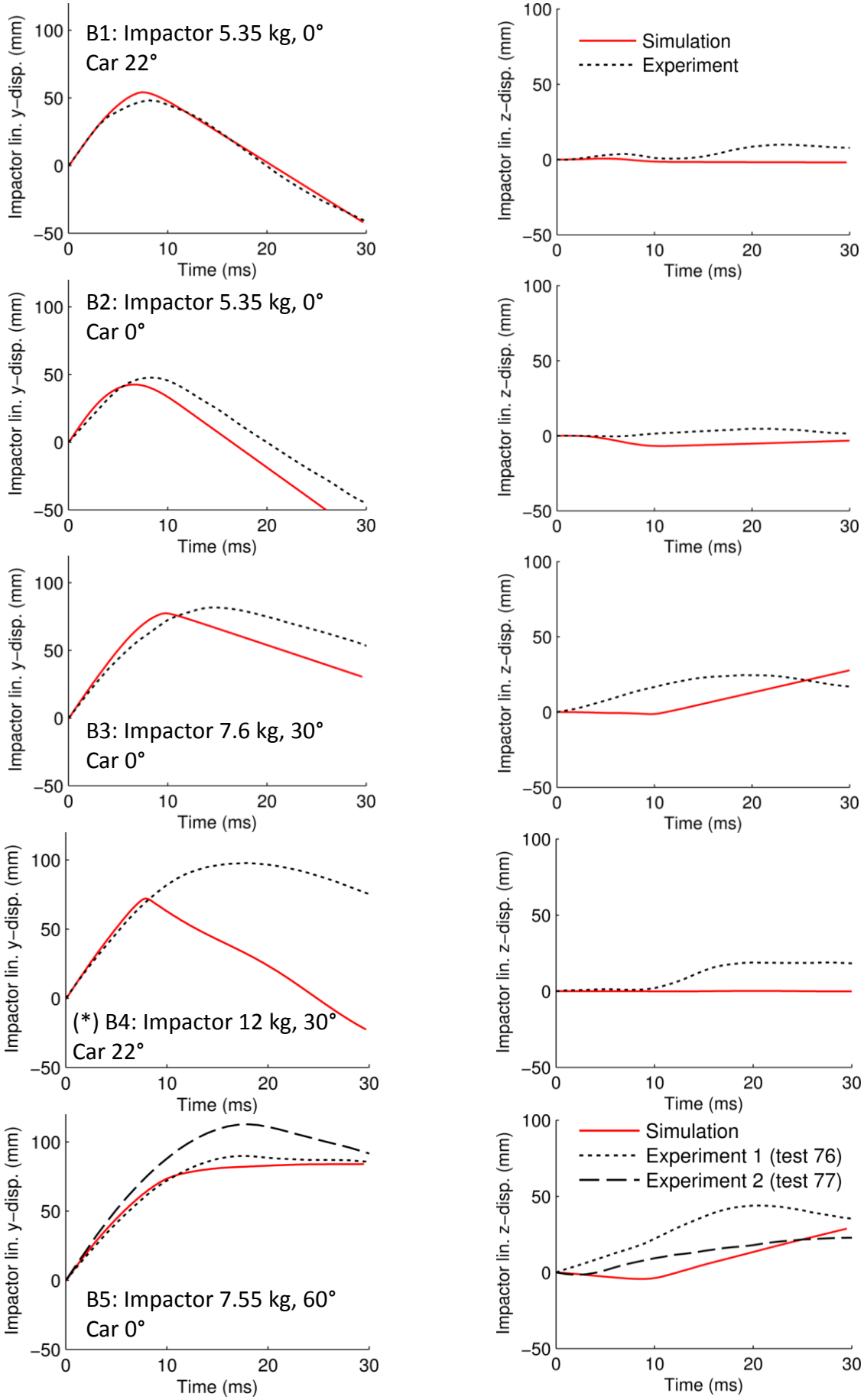

Fig. A-3. Results of validation test series B, leg impactor against vehicle front. (*) In test B4, measuring the unwanted movements in the experiment, the theoretical additional y-displacement of the impactor can be estimated by geometric calculation. The additional y-displacement estimated with this method is 21 mm, close to the actual difference of 25 mm between simulation and experiment.

Appendix B – Positioning in the experiments and simulations

In the experiments, positioning was aimed at a walking posture with the struck-side (right) leg slightly forward and the contralateral (left) leg slightly rearward. There was some variation in the initial stance of different subjects although the main differences were in the contralateral leg and contralateral arm (Table B-I).

TABLE B-I

MEASUREMENTS OF THE INITIAL POSTURES IN THE EXPERIMENTS AND SIMULATIONS. ANGLES WERE MEASURED CLOCKWISE (0° = VERTICAL AND 90° = HORIZONTAL). SHOULDER POSTURES AND HEAD ANGLES WERE NOT MEASURED BUT ESTIMATED BY OVERLAPPING SIDE-VIEW PRE-TEST PHOTOS WITH PICTURES OF MODEL POSTURES UNTIL THE POSTURES APPEARED TO MATCH. EACH OF THE MEASURED ANGLES IN THE SIMULATIONS WAS EQUAL IN ALL SCALING METHODS, E.G., THE THUMS RIGHT LOWER LEG ANGLE IN PM01 WAS THE SAME IN THE B, T1, T2, S3-S5 SIMULATIONS.

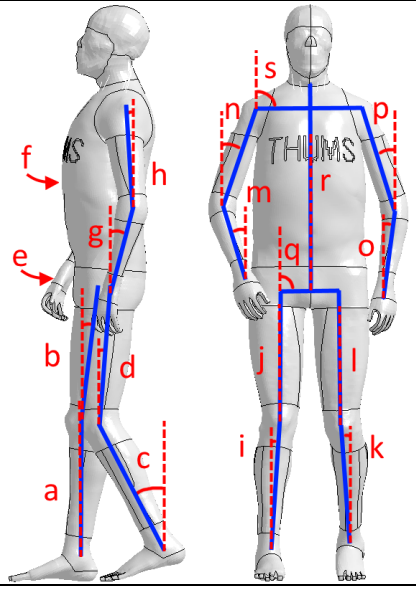

			PM01		PF02		PM03		PM04		PM05	
			Exp.	Sim.	Exp.	Sim.	Exp.	Sim.	Exp.	Sim.	Exp.	Sim.
Side view	*a*	*Right lower leg angle (°)*	-10	-5	-1	3	-12	-7	-8	-3	-3	-3
	b	*Right upper leg angle (°)*	6	6	7	-7	1	4	12	12	13	8
	c	*Left lower leg angle (°)*	-15	-11	-12	-9	-15	-10	-37	-34	-29	-28
	d	*Left upper leg angle (°)*	6	5	11	7	1	3	2	2	10	6
	e	*Right lower arm angle (°)*	4	9	10	14	9	12	14	15	12	17
	f	*Right upper arm angle (°)*	-8	-3	-2	-6	-1	3	-5	0	-1	-5
	g	*Left lower arm angle (°)*	44	41	17	20	22	25	32	31	11	14
	h	*Left upper arm angle (°)*	-1	-3	3	-1	8	11	1	3	4	4
Front view	*i*	*Right lower leg angle (°)*	1	-2	1	3	10	8	-6	-4	2	3
	j	*Right upper leg angle (°)*	-9	-7	0	1	8	7	1	2	4	1
	k	*Left lower leg angle (°)*	-8	-8	12	10	6	6	10	5	2	1
	l	*Left upper leg angle (°)*	-7	-6	-2	1	4	4	1	2	-4	-4
	m	*Right lower arm angle (°)*	-7	-2	2	-1	-10	-6	7	4	-10	-14
	n	*Right upper arm angle (°)*	9	9	8	8	7	9	5	7	15	18
	o	*Left lower arm angle (°)*	22	22	-3	1	12	10	13	12	8	7
	p	*Left upper arm angle (°)*	-25	-24	-8	-8	-4	-7	-5	-4	16	18
	q	*Pelvis angle (°)*	89	90	91	92	89	92	91	91	89	90
	r	*Upper body centreline angle (°)*	-1	-1	1	1	1	0	0	0	0	0
	s	*Shoulder angle (°)*	90	90	93	91	91	91	91	91	95	91

Appendix C – Detailed Results

In Appendix C, detailed results from the visual rating, head 6DOF kinematics from all experiments and simulations, and comparisons between scaling methods for head linear z-displacements (generally good CORA ratings) and head angular y-displacements (generally poor CORA ratings) are presented.

Appendix C1: Visual rating results

Detailed visual ratings are presented in Tables C-I – C-V. Results outside of the ranges specified in the method section are marked with (*). Elbow WAD was measured, but not taken into account for the visual rating since the exact value was not considered as important for head impact conditions as the other variables. Pictures of the elbow and head impacts in experiments and simulations are provided in Figures C1-C5.

TABLE C-I
VISUAL RATING DETAILS OF PM01 (WS = WINDSCREEN). RESULTS OUTSIDE OF THE REQUIRED RANGES ARE MARKED WITH (*)

	Exp.	b	t1	t2	s3	s4	s5
Pelvic sliding (cm)	25	23	20	23	16	17	22
Elbow abduction (°)	34	32	18	27	28	24	28
Elbow WAD	1640	1640	1490	1580	1540	1530	1570
Elbow response after impact	slipped away	stayed in place (*)	slipped away	slipped away	slipped away	slipped away	slipped away
Upper arm support	medium	strong (*)	medium	medium	medium	medium	medium
Head impact	WS	WS	WS	WS	WS	WS	WS
Total visual rating		poor	ok	ok	ok	ok	ok

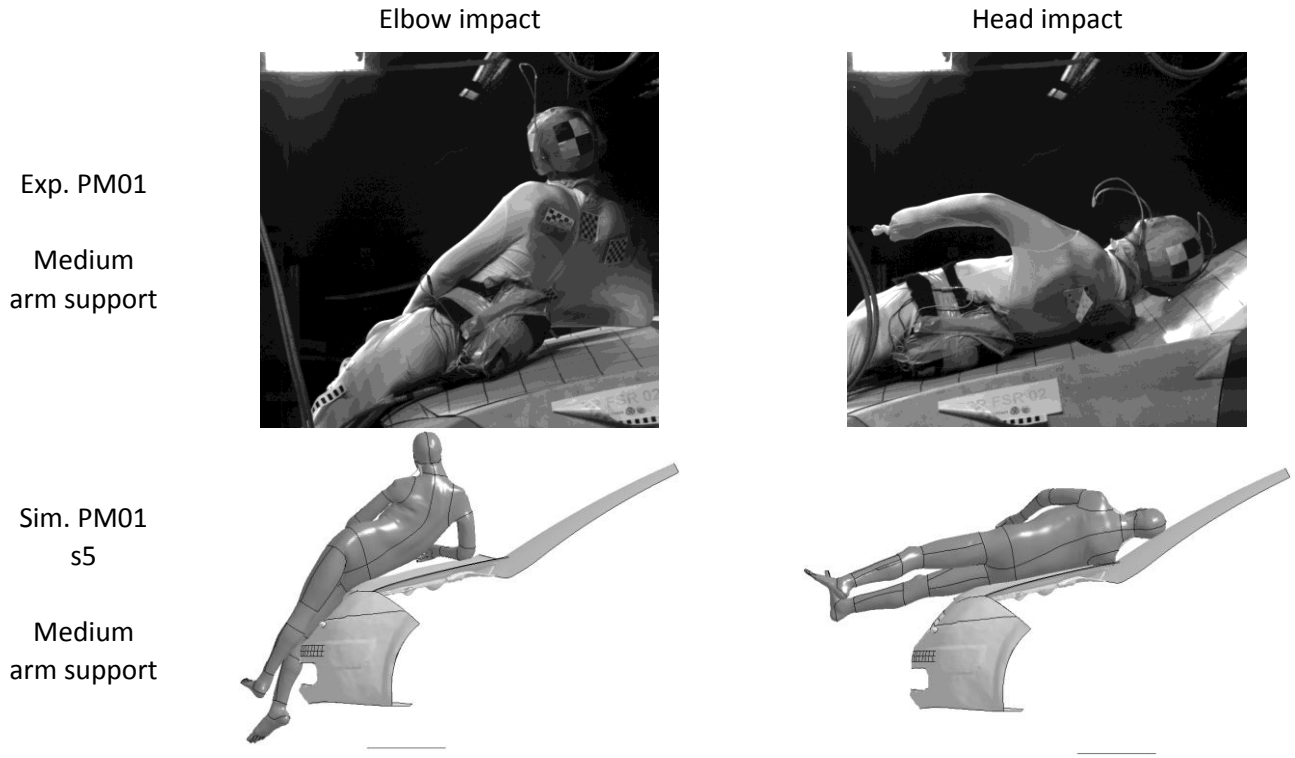

Fig. C1: Elbow and head impacts in experiment PM01 and simulation PM01-s5

TABLE C-II
VISUAL RATING DETAILS OF PF02 (WS = WINDSCREEN). RESULTS OUTSIDE OF THE REQUIRED RANGES LEADING TO MARGINAL OR POOR RATINGS ARE MARKED WITH (*)

	Exp.	b	t1	t2	s3	s4	s5
Pelvic sliding (cm)	0	16.5 (*)	0	20 (*)	11	13	9
Elbow abduction (°)	-16	26 (*)	-10	-4	-3	-2	-6
Elbow WAD	1250	1610	1070	1240	1230	1210	1260
Elbow response after impact	slipped away	slipped away	slipped away	slipped away	slipped away	slipped away	slipped away
Upper arm support	virtually none	medium (*)	virtually none	little	virtually none	little	virtually none
Head impact	bonnet	WS (*)	bonnet	WS (*)	bonnet	bonnet	bonnet
Total visual rating		poor	ok	poor	ok	ok	ok

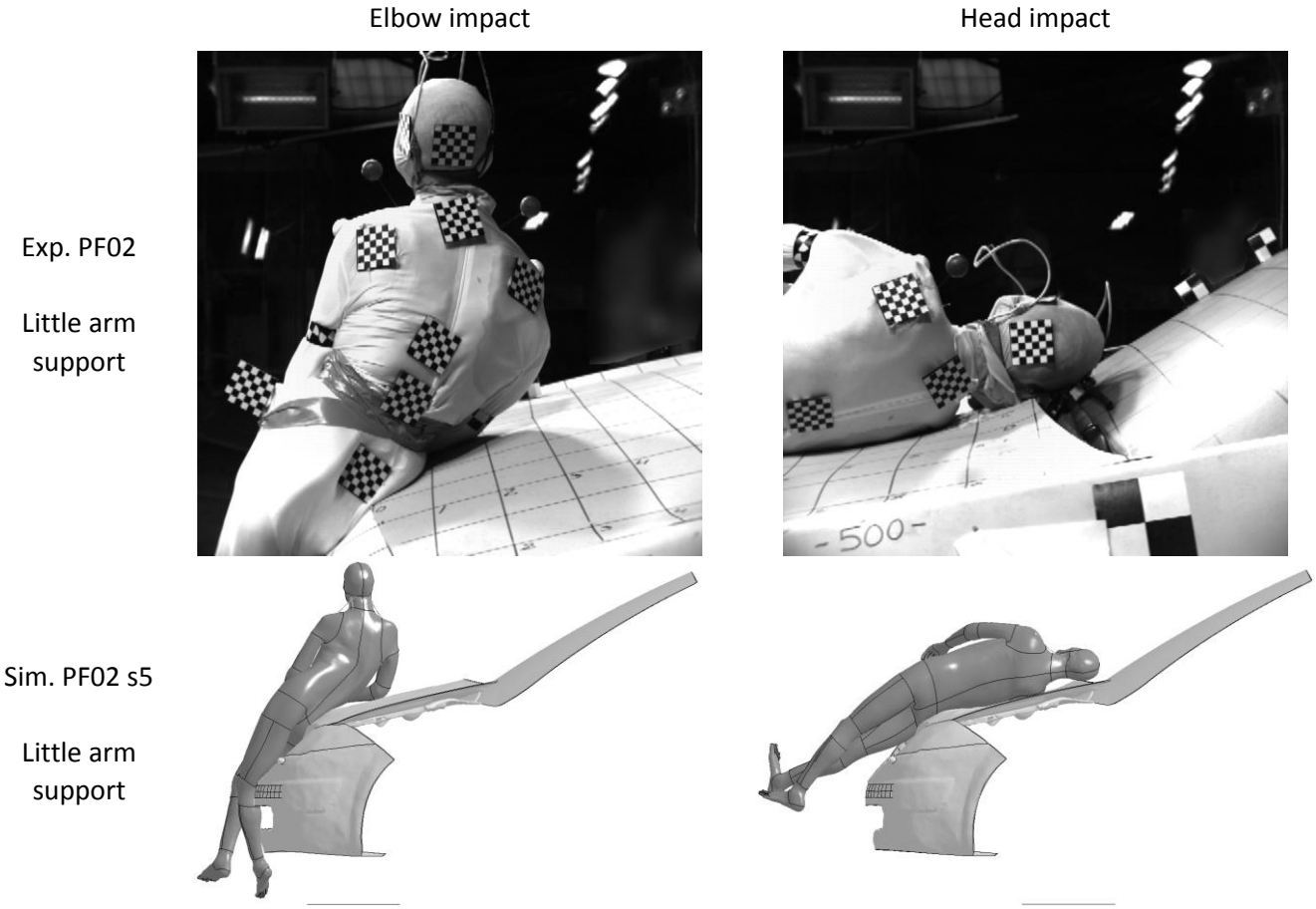

Fig. C2: Elbow and head impacts in experiment PF02 and simulation PF02-s5

TABLE C-III

VISUAL RATING DETAILS OF PM03 (WS = WINDSCREEN). RESULTS OUTSIDE OF THE REQUIRED RANGES LEADING TO MARGINAL OR POOR RATINGS ARE MARKED WITH (*). (**) PELVIC SLIDING WAS ALWAYS MEASURED UNTIL HEAD IMPACT TIME. IN SIMULATION S5, THE HEAD IMPACTED AFTER 138 MS WHEREAS IN THE EXPERIMENT, SLIGHT HEAD CONTACT STARTED 163 MS AFTER INITIAL CONTACT. IN THE EXPERIMENT, SLIDING AFTER 138 MS WAS 30 CM.

	Exp.	b	t1	t2	s3	s4	s5
Pelvic sliding (cm)	45 (**)	18 (*)	17 (*)	19 (*)	17 (*)	17 (*)	22 (*)
Elbow abduction (°)	73	27 (*)	28 (*)	24 (*)	27 (*)	25 (*)	29 (*)
Elbow WAD	1860	1580	1570	1610	1570	1590	1660
Elbow response after impact	stuck in WS	slipped away (*)	slipped away (*)	slipped away (*)	slipped away (*)	slipped away (*)	stuck in WS
Upper arm support	very strong	medium (*)	medium (*)	medium (*)	medium (*)	medium (*)	medium strong (*)
Head impact	none/WS	WS	WS	WS	WS	WS	WS
Total visual rating		poor	poor	poor	poor	poor	poor

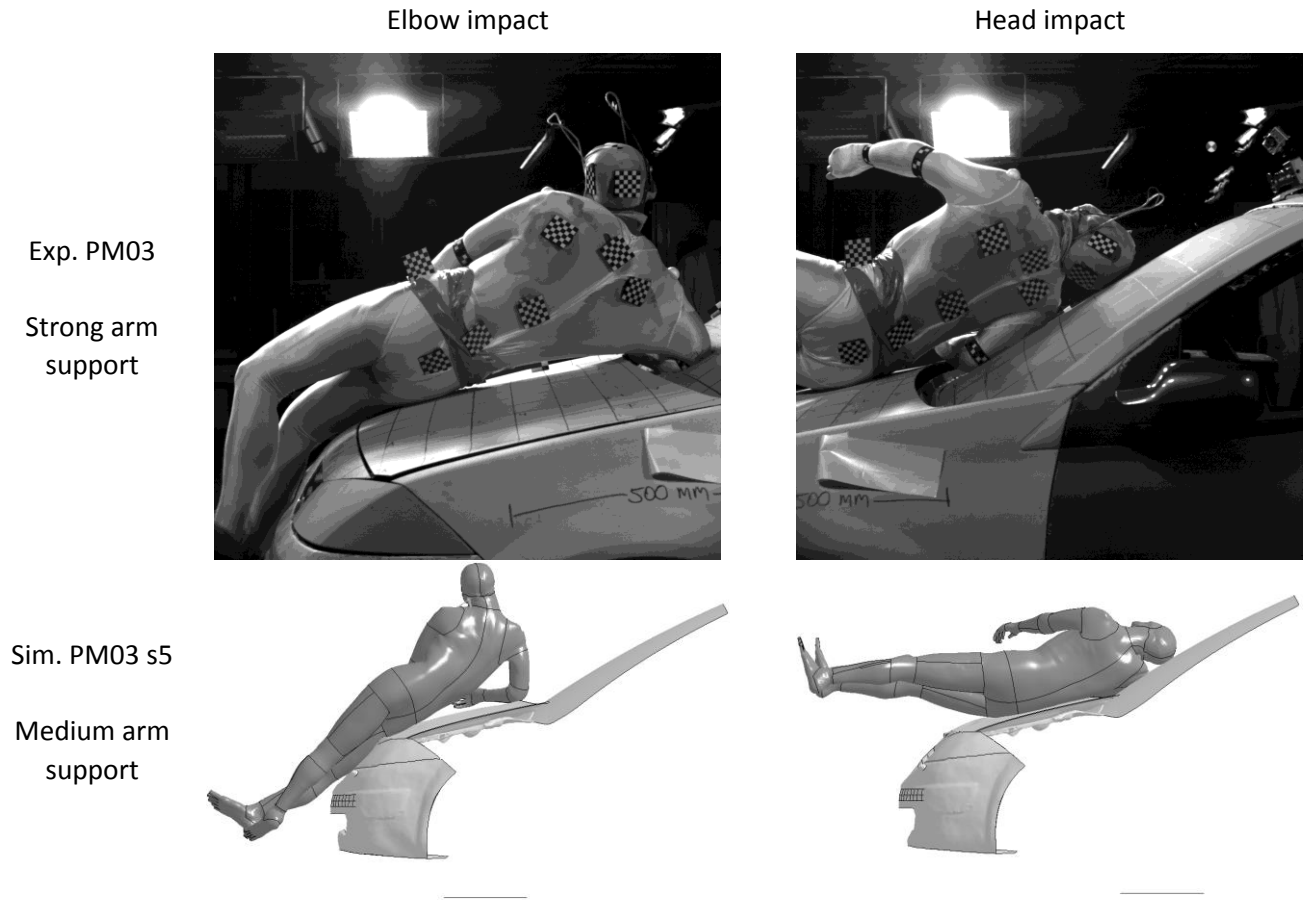

Fig. C3: Elbow and head impacts in experiment PM03 and simulation PM03-s5

TABLE C-IV
VISUAL RATING DETAILS OF PM04 (WS = WINDSCREEN). RESULTS OUTSIDE OF THE REQUIRED RANGES LEADING TO MARGINAL OR POOR RATINGS ARE MARKED WITH (*)

	Exp.	b	t1	t2	s3	s4	s5
Pelvic sliding (cm)	20	14	20	18	18	17	16
Elbow abduction (°)	8	13	8	10	11	9	12
Elbow WAD	1520	1490	1590	1530	1580	1570	1540
Elbow response after impact	slipped away	slipped away	slipped away	slipped away	slipped away	slipped away	slipped away
Upper arm support	medium	medium	medium	medium	medium	medium	medium
Head impact	WS	WS	WS	WS	WS	WS	WS
Total visual rating		ok	ok	ok	ok	ok	ok

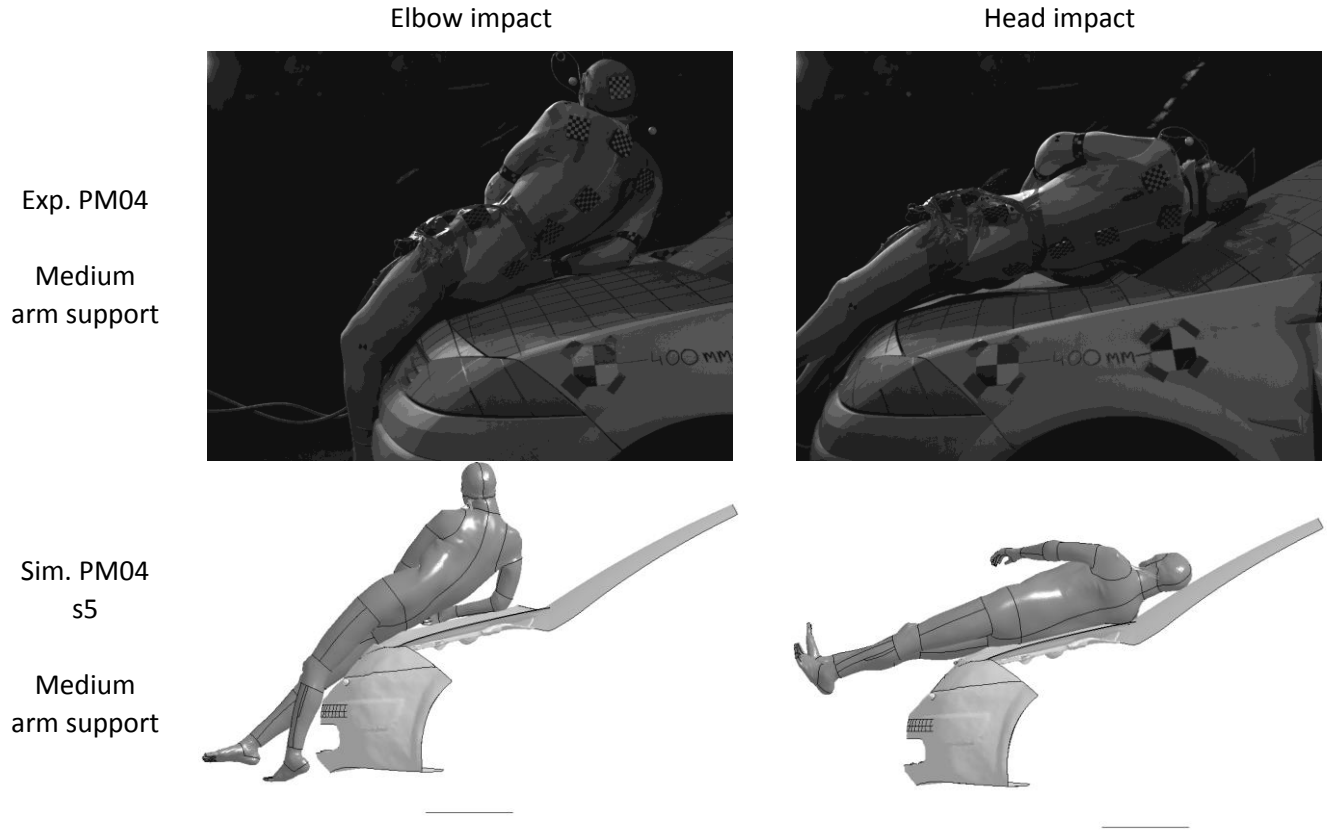

Fig. C4: Elbow and head impacts in experiment PM04 and simulation PM04-s5

TABLE C-V

VISUAL RATING DETAILS OF PM05 (WS = WINDSCREEN, FX = HUMERUS FRACTURE). RESULTS OUTSIDE OF THE REQUIRED RANGES LEADING TO MARGINAL OR POOR RATINGS ARE MARKED WITH (*)

	Exp.	b	t1	t2	s3	s4	s5
Pelvic sliding (cm)	25	17	15	14	15	17	16
Elbow abduction (°)	90	49 (*)	41 (*)	30 (*)	38 (*)	49 (*)	32 (*)
Elbow WAD	1750	1700	1640	1570	1640	1640	1560
Elbow response after impact	fx	fx	fx	fx	fx	fx	fx
Upper arm support	virtually none	little	little	little	little	little	little
Head impact	WS	WS	WS	WS	WS	WS	WS
Total visual rating		ok	ok	ok	ok	ok	ok

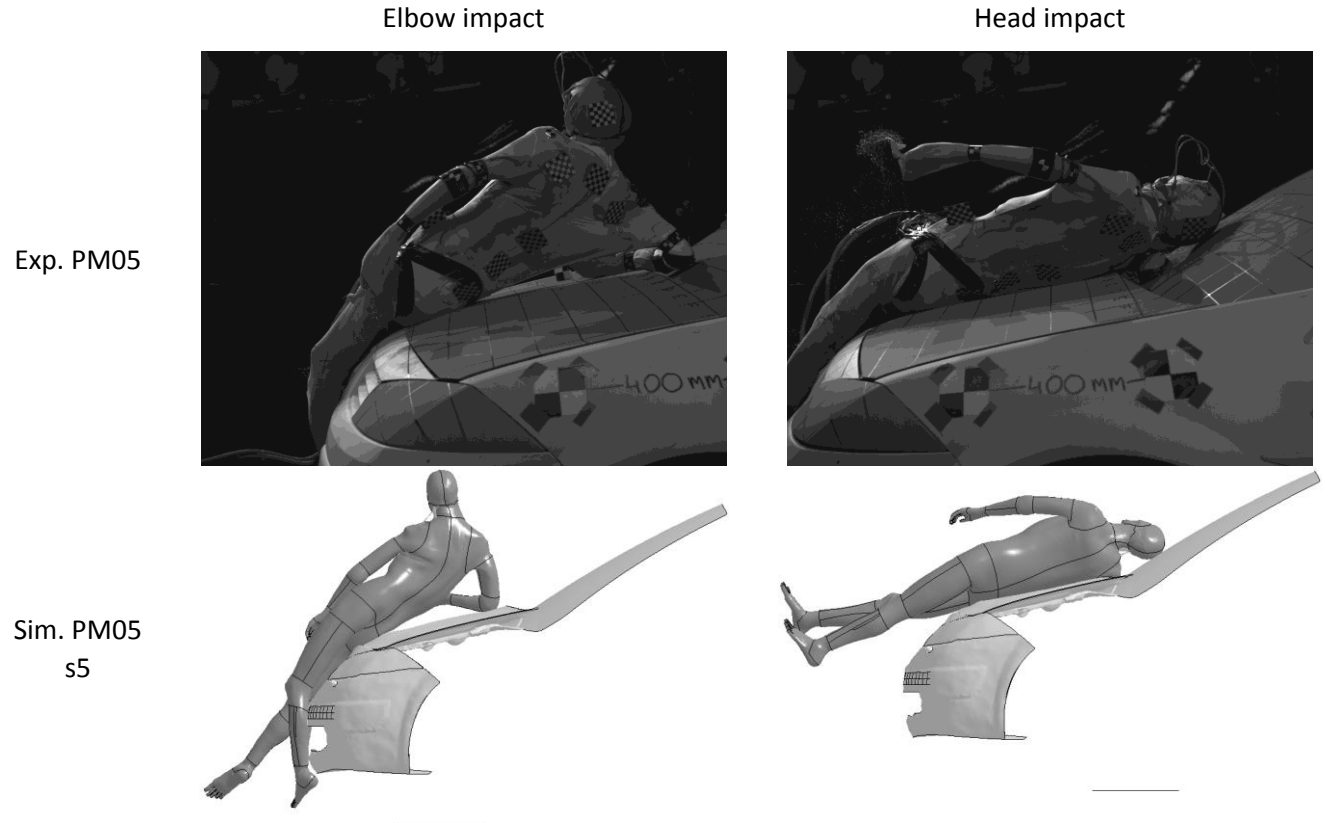

Fig. C5: Elbow and head impacts in experiment PM05 and simulation PM05-s5

Appendix C2: Head 6DOF displacements and velocities

Figure C-6 shows head 6DOF displacements, head resultant velocities and head angular x-velocities of all experiments and s5-simulations.

Head linear x-displacement was small for all tests and simulations. PM03 produced the largest head motion forward which THUMS did not reproduce. Head linear y-displacement in the global coordinate system was also rather small for PMHSs as well as in the simulations. The head linear y-displacement was smaller for shorter subjects and larger for taller subjects. Scaling THUMS using s5 also changed the linear y-displacement as a function of stature, but not as much as in the experiments. This could be due THUMS producing less head lag than observed in the PMHSs. Head downward motion started earlier for shorter than for taller subjects. With s5-scaling, these motions generally started slightly later than those of the experimental subjects.

Head angular x-displacements show that the head was first angled away from the vehicle starting after 50 ms for all experiments. THUMS did not reproduce this response in the s5 scaling; none of the simulations displayed head angulation away from the vehicle. The head angulation towards the vehicle then increased earlier for shorter subjects than for taller subjects. THUMS reproduced this difference to a larger extent; THUMS provided smaller angular displacements for subjects PM01 and PF02, but larger for PM03-PM05. Head angular y-displacements were mostly small in the experiments and the simulations. The experimental subjects PM01, PF02 and PM03 displayed slight neck flexion in the beginning which was later reduced. Subjects PM04 and PM05 displayed neck extension in the beginning which was later changed into neck flexion whereas THUMS only displayed slight neck flexion. Head angular z-displacement was mostly negative in the experiments and simulations, corresponding to neck lateral rotation with the face turning away from the vehicle. Subject PF02 was an exception displaying neck lateral rotation towards the vehicle instead which THUMS did not reproduce. THUMS angular z-displacements were generally smaller than those of the experimental subjects.

The resultant head velocity displayed a peak prior to head impact in all experiments and s5-simulations, followed by a more or less steep drop until first head-vehicle contact. In the experiments, the peak was highest in PM04 and PM05. In the simulations, the peak was higher than in the related experiments in PM01, PF02 and PM04 whereas it was smaller in PM03 and PM05. The head angular x-velocity in the experiments first displays a negative peak followed by a more extreme positive peak. PM03 displayed the highest peak. The simulated peaks were lower than the related experimental peaks in PM01, PF02 and PM03, and higher than the experimental peaks in PM04 and PM05. THUMS appears do provide rather similar peak head angular x-velocities independently of which experiment was simulated. Head rotational velocity is important in the prediction of brain injury risk; therefore, THUMS should better reproduce individual responses. This shortcoming was likely mainly due to different amounts of muscle tissue and strength in the PMHS necks which the scaling of THUMS did not individually account for. Although the two subjects with the most muscle mass were PM03 and PM04 which displayed the highest and the lowest peak of head angular x-velocity, PM03 displayed a very different response from all other subjects. For the remaining subjects, the peak was highest for the subject with the lowest amount of muscles and lowest for the subject with the highest amount of muscles. Future studies should look into how to individualise neck muscle strength in HBMs to better reproduce head angular x-velocity in full-scale pedestrian tests.

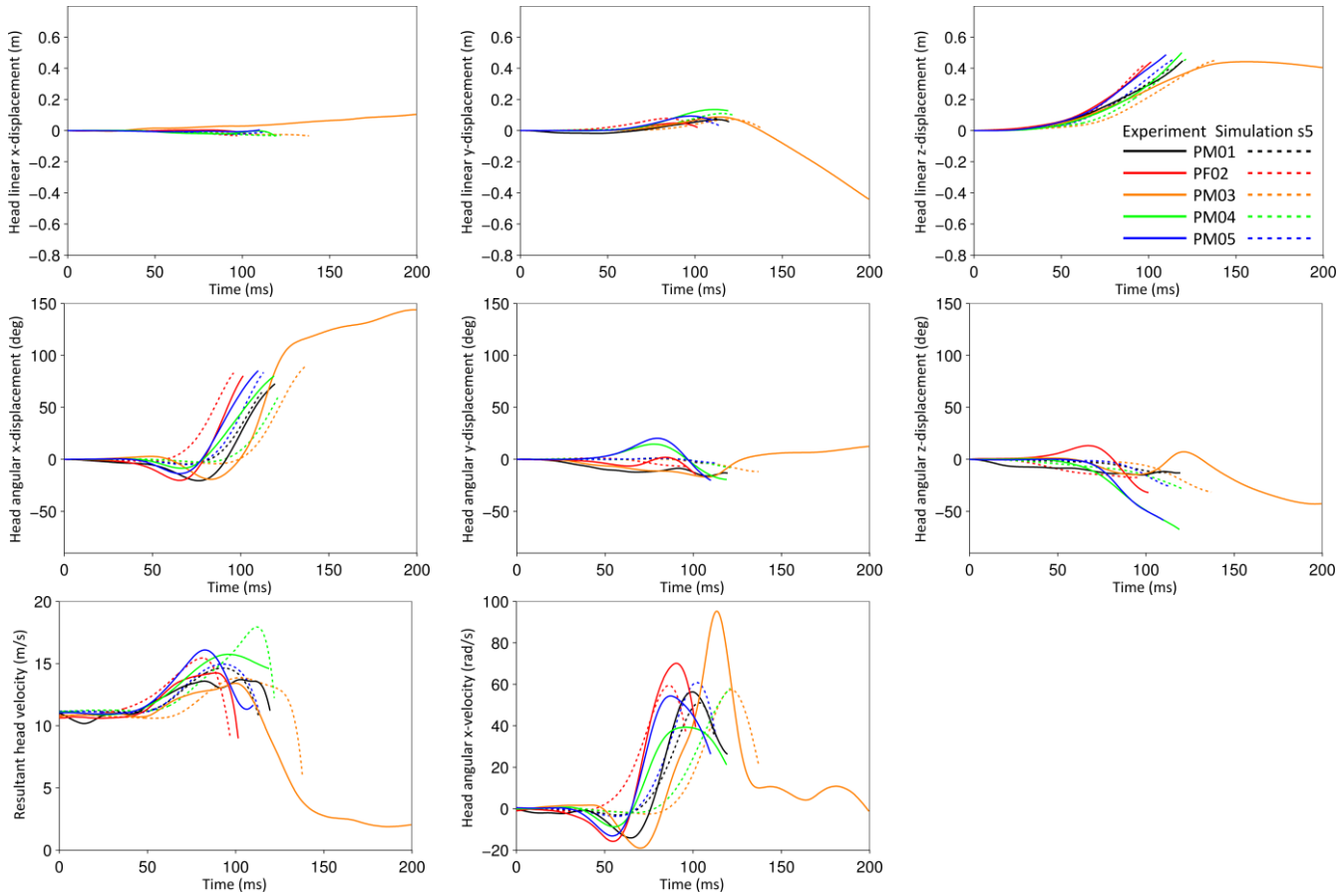

Figure C-6: Comparison of experimental and s5 simulation 6DOF head kinematics until head impact.

Figure C-7 shows head linear z-displacements (generally good CORA ratings) and angular y-displacements (generally poor CORA ratings) of each experiment compared with all related simulations.

Head linear z-displacements increased slightly more in the beginning of the experiments than in the beginning of the simulations for all scaling methods. In the later stages, the rate of descent was larger for the THUMS head than for that of the PMHSs. However, the head linear z-displacements were not strongly affected by the scaling method used. An exception was PF02 with scaling methods b and t2, where head linear z-displacement occurred later and the rate of descent was smaller than in the experiment. Head angular y-displacements were less pronounced in all simulations than in the experiments. The displacements generally started later in the simulations. A general trend with respect to scaling methods could not be observed in the head angular y-displacements.

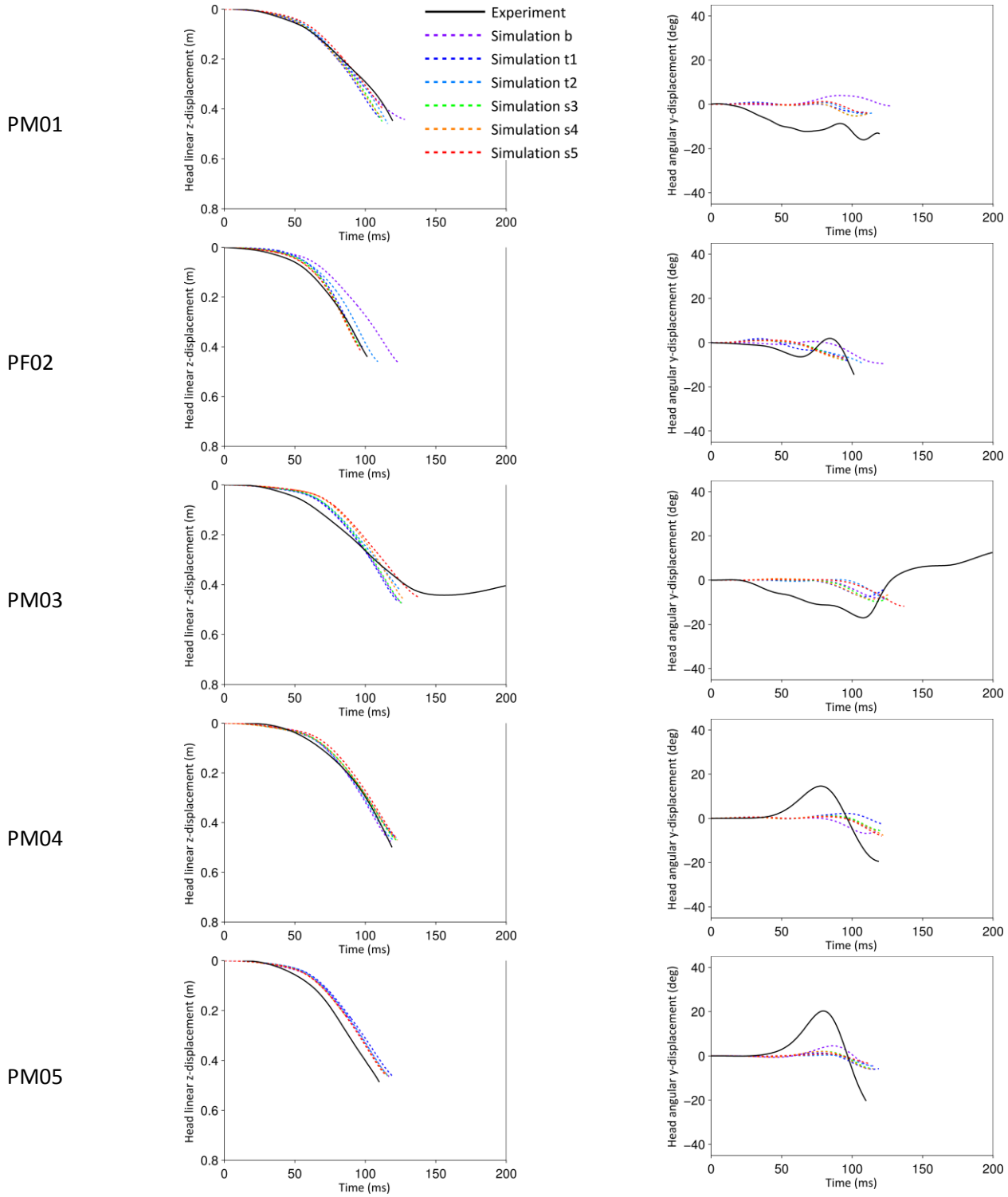

Figure C7: Comparison of experimental head linear z- and angular y-displacements with those recorded using different scaling methods.

Appendix C3: List of small and noisy experimental displacements

Several experimental displacements were small, i.e., below 0.1 m or 30° during the whole event (Table B-VI). Generally, head and spinal linear x-displacements as well as all angular y-displacements were small. Regarding linear y-displacements, it should be noted that these were occasionally small, but only in the global coordinate system. For head impact conditions and injury assessment, the vehicle coordinate system is more important.

TABLE C-VI
EXPERIMENTAL DISPLACEMENTS THAT WERE SMALL, I.E. BELOW 0.1 M OR 30° DURING THE WHOLE EVENT

	Experiment	Lin. x-disp.	Lin. y-disp.	Lin. z-disp.	Ang. x-disp.	Ang. y-disp.	Ang. z-disp.
	PM01	(NA)	small			small	small
	PF02	small	small			small	
Head	*PM03*	small	small			small	small
	PM04	small				small	
	PM05	small				small	
	PM01	(NA)				small	
	PF02	small				small	
T1/T2	*PM03*	small				small	small
	PM04	small	small			small	
	PM05	small				small	
	PM01	(NA)	small		small		small
	PF02	small					
T9/T11	*PM03*	small				small	
	PM04	small				small	
	PM05	small				small	
	PM01	(NA)	(NA)	(NA)	(NA)	(NA)	(NA)
	PF02	small	small	small		small	small
L2/L3/L4	*PM03*	small		small		small	
	PM04	small				small	
	PM05	small				small	
	PM01	(NA)	(NA)	(NA)	(NA)	(NA)	(NA)
	PF02	small		small		small	
Sacrum	*PM03*	small		small		small	
	PM04	small				small	
	PM05	small		small		small	
	PM01	(NA)	(NA)	(NA)	(NA)	(NA)	(NA)
	PF02			small	small	small	small
Pelvic H-p.	*PM03*					small	small
	PM04					small	
	PM05					small	
	PM01	(NA)	small		small		small
	PF02	small				small	
Acromion R	*PM03*					small	small
	PM04					small	
	PM05	small	small				
	PM01	(NA)	(NA)	(NA)	(NA)	(NA)	(NA)
	PF02	small	small				small
Acromion L	*PM03*	small					small
	PM04					small	small
	PM05	small				small	

Appendix D – Influence of Upper Arm Support

In some experiments and simulations, the upper arm visibly supported the upper torso and influenced the head kinematics prior to head impact against the vehicle whereas in others, there was little or no visible support. This behaviour was difficult to quantify directly, especially in the experiments where the load transmission from the humerus into the upper body was not recorded. Therefore, the upper arm support was assessed from a biomechanical perspective and through observation of how the elbow and upper arm response

influenced the upper torso and head kinematics in the experiments and simulations.

In this section, the effect of upper arm response on head impact velocities is analysed generally as well as in detail for experiments PM04 and PM05.

Appendix D1: General influence of upper arm support on the head impact velocities

As detailed in the Visual Rating paragraph in the Method section, the amount of humerus support provided to the upper torso was rated “none/little” when the arm was straight, the upper arm adducted or the humerus fractured upon elbow impact, “medium” when the upper arm was abducted but the elbow subsequently slipped away, or “strong” when the upper arm was abducted and the elbow stayed in place after impact. Such “strong” humerus support also resulted in motions of the shoulder towards the spine.

Figures C2 and C5 show four examples of the humerus support being rated as “none/little”. In experiment PF02, the arm was straight, i.e., there was little elbow flexion, due to the hand being caught between the subject and the vehicle upon pelvis impact. At the time of elbow impact, the upper arm was adducted instead of abducted as in the other experiments. Analysing the test video in detail, the upper arm was clearly not able to transfer a considerable amount of load into the upper torso in this position. In simulation PF02-s5, THUMS reproduced this behaviour. In experiment PM05, the PMHS suffered an anteriorly open comminuted humerus fracture shortly after elbow contact with the vehicle which was replicated in the simulations. Due to this fracture, the load transfer through the upper arm was clearly reduced (see also Fig. C5 and Appendix D3).

Medium support of the humerus to the upper torso was provided when the upper arm was abducted while the elbow impacted the bonnet, but then slipped away, as was the case in experiments PM01 and PM04 as well as in their s5-simulations (Fig. C1 and Fig. C4).

Strong humerus support was observed when the elbow did not slip away, but stayed in place. Fig. C3 (top) and Fig. D1 show two such examples. In experiment PM03, the elbow impacted the windscreen and dashboard where it was pinned. The upper arm then provided strong support to the torso which inhibited a typical, violent head impact against the vehicle. When PM05 was simulated without a humerus fracture, the t1-simulation displayed a similar behaviour. In this simulation, the elbow impacted the cowl panel between the bonnet and windscreen where its possibility to move was limited. Strong support from the upper arm then prevented a typical head impact in a similar way as in experiment PM03.

Appendix D2: Humerus abduction in PM04

In experiment PM04, a knot on the ipsilateral sleeve was caught between the subject and the vehicle between the time of pelvis impact and the time of elbow impact. The sleeve stretched while the upper arm abducted, but it limited the arm abduction. Simulations were carried out without and with reproducing the effect of the sleeve. When reproducing the sleeve, a spring was modelled attached to the wrist and the vehicle which produced a force of 200 N between the time of pelvis-vehicle contact and elbow-vehicle contact.

Without reproducing the effect of the sleeve, the upper arm abducted more than with the sleeve. Larger arm abduction generally produced more support for the upper torso after elbow impact. This support led to generally lower head impact velocities in the simulations in which the effect of the sleeve was not reproduced, compared with the simulations in which the effect of the sleeve was reproduced.

In the simulations where the sleeve was mimicked, the arm abduction was reproduced within 5°. However, head impact velocities were still over 12 % smaller than in the experiments.

TABLE D-I
HEAD IMPACT VELOCITY RESULTS FOR PM04 WITH AND WITHOUT SIMULATED SLEEVE. HEAD IMPACT VELOCITY IN THE EXPERIMENT WAS 14.54 M/S

Scaling	With simulated sleeve		Without simulated sleeve	
	m/s	%	m/s	%
b)	8.53	-41.3	8.94	-38.5
t1)	10.56	-27.4	9.90	-31.9
t2)	10.55	-27.5	8.23	-43.4
s3)	9.46	-34.9	8.81	-39.4
s4)	10.95	-24.7	6.29	-56.8
s5)	12.73	-12.5	NA	NA

Appendix D3: Humerus fracture in PM05

To investigate the influence of the humerus fracture in PM05, three sets of simulations were run, one with a fracture at the time of first elbow contact with the vehicle, one with a fracture 5 ms after first elbow contact as observed in the experiment, and one with no fracture at all.

When the fracture was not at all simulated, the simulations predicted head impact velocities that were consistently far lower than in the experiment (Table D-II). In two of the simulations without fracture, t1 and s3, the upper arm provided strong support to the upper torso which resulted in very low head impact velocities (Fig. D1). The head impact velocity prediction improved when a fracture was simulated 5 ms after elbow contact. Simulating the fracture at an earlier point in time resulted in lower head impact velocities. The earlier fracture led to the upper arm not slipping away to the same extent as in the later fracture. Thus, the upper arm provided more cushioning to the upper torso which led to generally lower head impact velocities compared with the simulations where the fracture occurred slightly later.

TABLE D-II
HEAD IMPACT VELOCITY RESULTS FOR PM05 WITH AND WITHOUT SIMULATED FRACTURE. HEAD IMPACT VELOCITY IN THE EXPERIMENT WAS 11.83 M/S

Scaling	No fracture		Fracture 5 ms after elbow contact		Fracture at elbow contact	
	m/s	%	m/s	%	m/s	%
b)	7.64	-35.4	9.78	-17.3	NA	NA
t1)	1.58	-86.6	8.25	-30.2	7.36	-37.8
t2)	5.99	-49.4	11.17	-5.6	7.30	-38.3
s3)	1.01	-91.5	8.42	-28.8	7.83	-33.8
s4)	NA	NA	10.60	-10.4	7.75	-34.5
s5)	6.99	-40.9	11.00	-7.0	7.53	-36.4

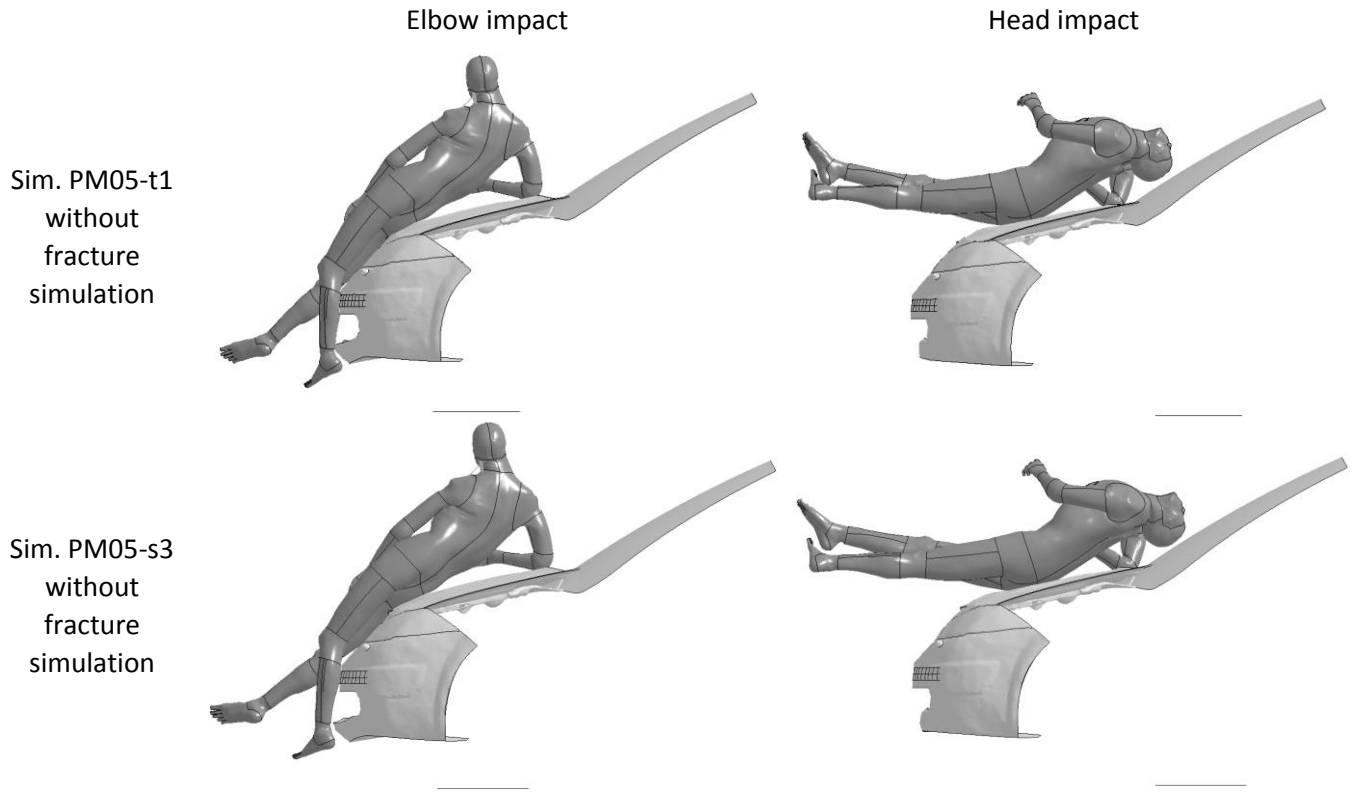

Fig. C1: Strong humerus support led to very low head impact velocities in simulations PM05-t1 and PM05-s3 when no fracture was simulated.